Bottom-up vs top-down drivers of eruption style: Petro-geochemical constraints from the holocene explosive activity at La Soufrière de Guadeloupe

Abigail Metcalfe, Séverine Moune, Jean-Christophe Komorowski, Roberto Moretti

Bottom-up vs Top-down Drivers of Eruption Style: Petro-Geochemical Constraints from the Holocene Explosive Activity at La Soufrière de Guadeloupe

Abigail Metcalfe[1*], Séverine Moune[1,2,3], Jean-Christophe Komorowski[1], Roberto Moretti[1,2]

[1] Université de Paris, Institut de physique du globe de Paris, CNRS UMR 7154, F-75005 Paris, France

[2] Observatoire volcanologique et sismologique de Guadeloupe, Institut de physique du globe de Paris, F- 97113 Gourbeyre, France.

[3] Laboratoire Magmas et Volcans, OPGC, Clermont-Ferrand, CNRS UMR 6524

*metcalfe@ipgp.fr

Abstract

Signals of volcanic unrest have been used successfully to provide insights into the timing, magnitude, intensity, and style of future eruptions. However, in order to provide context for the subsequent activity analysis of past eruptions is required. This provides useful information in order to understand processes of magma genesis, storage, evolution and ascent which lead to the onset of future eruptions. Here, we examine basaltic-andesitic to andesitic deposits from La Soufrière de Guadeloupe Holocene eruptions, covering a range of explosive eruption styles, ages and magnitudes. Our work is timely given unrest at this system has increased over the last 25 years, with a potential eruption capable of directly impacting up to 80,000 people in Southern Basse-Terre and potentially thousands more indirectly on a regional scale. We report on the geochemistry of pre-eruptive magmas using detailed analyses of glass (melt inclusions and groundmass glass) from four Holocene explosive eruptions: 1657 Cal. CE (Vulcanian, VEI 2), 1530 Cal. CE (sub-Plinian, VEI 3), 1010 Cal. CE (Plinian, VEI 4), and 5680 Cal. BCE (Plinian, VEI 4). Major element concentrations vs SiO_2 in whole rock (WR), groundmass glass (GM) and melt inclusions (MI) show a strong linear trend. MIs reveal a relatively homogenous melt composition from the first to the most recent eruptions, ranging from 63.6 – 78.7 wt% SiO_2. Volatiles, including H_2O (2.3 - 4.4 wt%), CO_2 (35 - 866 ppm) and sulphur (30 - 202 ppm), are also consistent across the various eruptions. The major element and volatile compositional homogeneity across the eruptions indicates that composition and volatiles do not have a direct control on eruption explosivity at this system. Instead, we find differences in ascent rate, groundmass glass viscosity and microlite volume percentage indicating that explosive eruptive style at La Soufrière is controlled by a combination of ascent rate and top-down controls affecting rock strength, stress distribution and the development of fluid overpressure. Rapid ascent in the absence of top-down controls (processes with a cause external to the magma but affecting the plumbing system) will result in explosive eruptions driven from the bottom-up (internal to magma dynamic response with varying pressure and temperature, e.g., 1010 Cal. CE in the case of very rapid ascent or 1657 Cal. CE in the case of rapid ascent). However, we also highlight the importance of top-down controls such as conduit sealing which can promote

the onset of explosive eruptions, even in the case of slow magma ascent (e.g., 5680 Cal. BCE). External effects (including ingress of water and rapid edifice unloading) can also favour explosive eruptions with flank collapses involved in some scenarios (e.g., 1530 Cal. CE). The multiple controls on explosive eruption style make this system more hazardous and complex to model and monitor. In order to improve early-warning system efficiency, forecast models, eruption scenario crisis response and long-term risk reduction planning, we stress that internal processes such as fracture and host-rock sealing (fluid pore pressure) as well as external processes such as water moving into the system and the mechanical stability of the edifice should be monitored and modelled closely.

Keywords: Eruption style, melt inclusions, ascent rate, mixing and mingling, La Soufrière de Guadeloupe

1 Introduction

Eruption style dictates many of the hazards presented by a volcano, however, volcanoes are not limited to one particular eruption style. Changes in eruption style can occur over short periods e.g., multiple transitions within a single eruptive episode (e.g., Cioni, et al., 2008; Boudon et al., 2008) and long periods e.g., different eruption styles separated by a repose period (e.g., Endo et al., 1981; Ratdomopurbo et al., 2013; Costa et al., 2013). In particular, explosive eruptions are hazardous and can range in style at one system from small Vulcanian activity to large sub-Plinian and Plinian activity (e.g., Soufrière Hills Volcano, Montserrat, (Komorowski et al., 2010; Wadge et al., 2014); La Soufrière de Guadeloupe (Komorowski et al., 2005; Legendre, 2012); Etna, Italy (Coltelli et al., 2005; Moretti et al., 2018; Cappello et al., 2019); Rabaul, Papua-New-Guinea (Bernard and Bouvet de Maisonneuve, 2020)).

Current volcano monitoring, such as geochemical and geophysical methods, can provide indications of volcano activity and the onset of unrest (e.g., Gottsman et al., 2019; Pritchard et al., 2019). However, in order to provide a more complete picture, understanding the controls on eruptive style, and particularly the controls on transitions between styles is required to develop realistic eruption scenarios.

There are multiple ways to generate a magmatic, explosive eruption: (1) heating of the system causing magma convection and vesiculation (Sparks, et al 1977; Melnik and Sparks, 1999) and/or the mobilization of crystal-rich magmas (Burgisser and Bergantz, 2011; Andrews and Manga et al., 2014); (2) addition of magma volume into the system which increases the overpressure on the confining walls (Ruprecht and Bachmann, 2010; Bouvet de Maisonneuve et al., 2013; Degruyter, et al 2016); (3) effective degassing of volatile rich magma and volatile fluxing which increases buoyancy and overpressure during ascent (Roggensack et al., 1997; Scandone et al., 2007; Helo et al., 2011; Sides et al., 2014; Costa et al., 2013; Parmigiani et al., 2016; Edmonds and Wallace, 2017); (4) rapid magma ascent rate preventing efficient gas–melt segregation (e.g., Gonnermann and Manga, 2007; Goepfert and Gardner, 2010; Martel, 2012; Lloyd at al., 2014; Barth et al., 2019); (5) syn-eruptive

microlite growth resulting in an increase in magma viscosity (e.g., Houghton & Gonnermann, 2008; Moitra et al., 2018; Arzilli et al., 2019; Hlinka, 2020; Hlinka et al., 2021), (6) increased mechanical connectivity by shallow level volcanic seismic rupturing (Roman and Cashman, 2018). These processes are likely to occur combined in order to produce magma fragmentation and explosive eruptions (Gonnermann and Manga, 2007; Cassidy et al., 2018; Hlinka, 2020; Hlinka et al., 2021).

At subduction zones transition in eruption style is common, with transitions observed within the same eruption (e.g., effusive to explosive) and across several eruptions with an observed repose period (Cassidy et al., 2018). The range of eruption styles observed at such systems makes them particularly hazardous and defining the processes and controls on each eruption style is particularly important. In recent years the interplay of bottom-up (internal to magma dynamic response with varying pressure and temperature) vs top-down (processes with a cause external to the magma but affecting the plumbing system) has been shown to play an important role in triggering transitions in eruption style (e.g., Sparks, 1997; Cassidy et al., 2018; Bernard and Bouvet de Maisonneuve, 2020).

Bottom-up processes drive an eruption through physico-chemical changes which are intrinsic in the magma system (e.g., crystallisation, degassing and chemical differentiation, mixing of other magmas) and control magma rheology. These processes affect magma properties, and therefore affect magma migration in the crust and ascent and decompression rates, key parameters in determining eruption style, particularly the explosive one via the onset of fragmentation (Dingwell, 1996; Alidibirov and Dingwell, 1996; Gonnermann, 2015 and refs. therein). For a given felsic magma composition the total amount of volatiles in the system and the composition of the melt itself, are critical parameters in determining fragmentation thresholds and explosivity (e.g., Papale, 1999; Di Genova et al., 2017).

Top-down processes may involve non-magmatic causes and sources, related to water circulation and gravity or be the result of magma evolution in conduits. Rapid and efficient infiltration of external waters can lead to phreato-magmatism (Zimanowski et al., 2015); over a longer-term, water circulation promotes rock alteration and secondary mineral precipitation in the presence of well-developed hydrothermal systems (e.g., Barberi et al., 1992; Roman et al., 2019; Stix & de Moor, 2018). Top-down processes may greatly modify the edifice stability and rock, strength, and/or promote fluid overpressure. In all cases they alter the stress distribution within the volcanic edifice, particularly in the upper portion at shallow depths.

Gravity-induced instabilities can determine sudden changes to the edifice e.g., flank collapse or dome collapse resulting in a downward-propagating decompression wave which triggers magma fragmentation (e.g., Voight et al., 1981; Sparks et al., 2002; Alidibirov and Dingwell, 1996; Komorowski et al., 2013). On longer timescales, volcano spreading was recognized to decrease thresholds for the occurrence of highly-explosive Plinian eruptions (Borgia et al., 2005).

Top-down controls resulting from magma evolution in conduits involve sealing of the upper portions of a plumbing system, which results from rapid thermal exchange due to a high surface/volume ratio when magma supply is low or nil and degassing-induced crystallization is high (De Natale et al., 2004; Quareni et al., 2007). Concomitant but external factors contributing to conduit sealing are plugging due to collapse (particularly at calderas) and the rock overburden pressure, which the tectonic regional stress can contribute to either positively (compressive) or negatively (tensile) (Quareni and Mulargia, 1993). Changes that occur in the uppermost plumbing system affect late-stage decompression path of magma considerably and control eruption style from the top-down (Thomas and Neuberg 2014, Cassidy et al., 2018). An open conduit, or one which is not sealed effectively, will allow magma to lose gas efficiently making an effusive eruption likely (Sparks, 1997). In comparison, a sealed system may lead to pressure build-up due to deep degassing and prime the volcano for an explosive eruption (Sparks, 1997; Komorowski et al., 1997; Burgisser et al. 2011; Preece et al., 2016; Roman et al., 2019; Komorowski et al., in prep). This indicates the role of bottom-up and top-down processes can cause transitions in eruptive behaviour both during a single eruption and across multiple eruptions.

In this study we focus on understanding the variability in explosive eruption style over several eruptions occurring within a period of ca. 7000 years. For this purpose, we study four eruptions from La Soufrière de Guadeloupe: the 5680 Cal. BCE Plinian eruption (VEI 4), the 1010 Cal. CE Plinian eruption (VEI 4), the 1530 Cal. CE sub-Plinian eruption (VEI 3) and 1657 Cal. CE Vulcanian eruption (VEI 2). We use the chemical composition and volatile content of volcanic glass (melt inclusions and groundmass glass) to understand how the magmatic parameters such as, the pre-eruptive magma composition, conditions and physicochemical parameters in the conduit relate to variations in eruption styles.

2 Geological and Magmatic Setting

2.1 Eruptive History

Guadeloupe is found in the central Lesser Antilles arc and formed as a result of subduction of the Atlantic plate beneath the Caribbean plate. Basse-Terre, the western island of Guadeloupe, was formed over the last ca. 3 million years by the active inner volcanic arc which has produced several volcanic complexes (Komorowski et al., 2005; Samper et al., 2007). La Soufrière de Guadeloupe Volcano (hereby referred to as La Soufrière) is part of the most recently active Grande-Decouverte-Soufrière complex (Fig 1). Ca. 80,000 people live in the south of Basse Terre and would be impacted by a future eruption of La Soufrière eruption (Komorowski et al., 2005; Leone et al., 2019; Esposti Ongaro et al., 2020).

La Soufrière is a basaltic-andesite to andesitic arc volcano built over the older Monts Caraïbes complex and has been active since ca. 7140 Cal. BCE until present day (Legendre, 2012; Komorowski et al., 2005; 2012; 2013). A large variation in magmatic eruption styles are observed at this system, from effusive dome building eruptions to explosive behaviour

ranging from Vulcanian to Plinian eruptions (Komorowski et al., 2005; Boudon et al., 2008; Legendre, 2012; Komorowski et al., 2013).

At La Soufrière two types of transitions between magmatic eruption styles are observed: (1) a transition in eruption style within the same eruption (e.g., 1530 Cal. CE which had explosive sub-Plinian and strombolian phases followed by an effusive dome building phase (Boudon et al., 2008; Komorowski et al., 2008), (2) a transition in eruption style over several eruptions with an observed repose period (e.g., the La Soufriere eruptive record shows individual eruptions separated a repose period ranging from Plinian to Vulcanian to effusive eruptions (Komorowski et al., 2005; Legendre, 2012).

Since 1635 Cal. CE, the majority of historic activity at La Soufrière has been phreatic (Feuillard et al., 1983; Komorowski et al., 2005), related to the well-developed hydrothermal system. Recent unrest at the system has suggested the movement and emplacement of magma at depth (Moretti et al., 2020) triggering pulses of recurrent heating and pressurisation of the hydrothermal system. However, there are few constraints on the controls of eruption style at this system and the transitions between eruption styles are poorly understood.

The eruptions presented in this paper cover the variety of explosive eruption styles which have occurred at La Soufrière through the Holocene, a full eruptive history is detailed in Komorowski et al. (2005); Legendre (2012) and Metcalfe et al. (2021). Four eruptions are discussed in detail: 5680 Cal. BCE, 1010 Cal. CE, 1530 Cal. CE and 1657 Cal. CE.

The 5680 Cal. BCE eruption is a Plinian eruption (VEI 4) and was the first explosive and most violent eruption preserved in the La Soufrière record. The 1010 Cal. CE eruption is the most recent Plinian eruption (VEI 4). The most well studied, archetypal eruption of La Soufrière is the multistage eruption of 1530 Cal. CE, that started with an edifice collapse phase, evolved into an explosive sub-Plinian (VEI 3) phase and ended with the growth of the current dome (Komorowski et al., 2005; Boudon et al., 2008; Komorowski et al., 2008; Esposti Ongaro et al., 2020). Finally, the last magmatic eruption was the 1657 Cal. CE a Vulcanian eruption (VEI 2-3) (Komorowski et al., 2012; 2013; Legendre, 2012; Metcalfe et al., 2020). We also discuss basaltic samples from the Monts Caraïbes complex, which is found in the southernmost part of Basse-Terre and erupted between 555 ± 26 and 472 ± 16 ka (Blanc, 1983; Fig. 1). The least evolved magmas observed on Basse-Terre were produced during this phase, with the Monts Caraïbes magma often hypothesised as the parental magma from which other magmas on the island evolved (Bissainte, 1995).

Currently, La Soufrière has a developed hydrothermal system and following the 1657 Cal. CE eruption, only phreatic/hydrothermal eruptions have occurred, with the last event in 1976-1977 (Feuillard et al., 1983; Komorowski et al., 2005). This eruption resulted in the evacuation of >70,000 people from Basse-Terre (Le Guern et al., 1980; Feuillard et al., 1983; Hincks et al., 2014) and resulted in increased monitoring of this system. The peak of recent unrest occurred in April 2018 when a M4.1 earthquake was recorded, this was the

strongest seismic event since 1976-1977. This is interpreted to relate to a failed phreatic event (Moretti et al. 2020).

2.2 Magmatic System

Models of the La Soufrière system involve the storage of a parental magma in a deep, zoned magma chamber below a system comprised of shallow-depth crystallised intrusions, as proposed by Touboul et al. (2007) and later by Pichavant et al. (2018). In both models the shallow andesitic system is remobilised by mafic magma moving up from the deeper system.

More recently, a mush system has been proposed for the structure of the La Soufrière magmatic reservoir (Moretti et al., 2020; Metcalfe et al., 2021). Mush systems are long-lived storage zones and are located at variable depths in the crust. These systems are composed of crystal and melt lenses in variable states of cooling and are built by repeated intrusions from depth (e.g., Mahood, 1990; Nakamura, 1995; Bachmann et al; 2002; Zellmer et al., 2003; Moretti et al., 2013, 2019; Brown et al., 2014; Cooper and Kent 2014; Annen et al., 2015; Bergantz et al., 2015, 2017; Edmonds et al., 2016; Cashman et al., 2017; Spera and Bohrson, 2018; Carrara et al., 2019). Crystals in the mush system have close contacts which form a continuous interlocking framework, through which melt is distributed in varying volumetric proportions and in variable states of eruptibility (e.g., varying temperature, density, viscosity, volatile content) (Cashman et al., 2017; Spera and Bohrson, 2018).

At La Soufrière, the mush lenses are hypothesised to vary through the reservoir with different lenses hosting different crystal populations (Metcalfe et al. 2021). This results from repeated intrusions interacting with the lenses differently due to the intrusion's size, geometry and location as well as physio-chemical properties (Metcalfe et al. 2021).

Melt and/or fluid migration, amalgamation and mixing render the system inherently unstable allowing remobilisation through disaggregation of the mush lenses (Costa et al., 2009; Mader et al., 2013; Rubin et al., 2017; Cooper and Kent, 2014; Sparks and Cashman, 2017; Jackson et al 2018; Cooper 2019). At La Soufrière, it is hypothesised that magma recharge leads to remobilisation of magma mush (e.g., Bergantz et al., 2015, 2017; Schleicher et al., 2016; Schleicher and Bergantz 2017). Recharge may not result in remobilisation of the whole system, and only small areas may remobilise depending on intrusion geometry which relates to density differences between the intruding magma and host mush (Bergantz et al., 2015, 2017; Schleicher et al., 2016; Schleicher and Bergantz 2017). This remobilised area may differ between eruptions, meaning not all the crystals interact with the same amount of intruding magma, therefore allowing different populations of crystals to be involved in different eruptions (Carrara et al., 2019; Cheng et al., 2020; Metcalfe et al. 2021).

The pre-eruptive melt composition is well constrained for the 1530 Cal. CE eruption (Poussineau, 2005; Boudon et al., 2008; Pichavant et al., 2018). Two magma compositions were involved to form the archetypal 1530 Cal. CE banded eruption products. This resulted

in a wide range of whole rock (WR) compositions observed from 55 - 62 wt% SiO_2 (Semet et al., 1981; Boudon et al., 2008; and Pichavant et al., 2018). However, the hybrid magma composition is not reflected in melt inclusions (MI), with inclusions from both mafic and silicic andesite bands falling in the range 70.5 – 78.7 wt% SiO_2 (Poussineau, 2005; Boudon et al., 2008 and Pichavant et al., 2018). Groundmass glass (GM) do reflect this hybrid composition, with the most silicic GM found in the homogenous andesitic pumice and white layers of the banded pumice, whereas more mafic glass is found in dark pumice bands. This indicates that the La Soufrière reservoir hosts an evolved melt composition and that recharge from depth, as in the case of the 1530 Cal. CE eruption, is more mafic with respect to the magma in the reservoir.

Quantification of MI concentrations and experimental data from 1530 Cal. CE MI studies by Pichavant et al. (2018) allows a pressure of 170 MPa for the source of this eruption to be constrained This also allows a minimum depth for the top of the La Soufrière magma reservoir to be constrained between 5.6 and 7.1 Km. The absence of amphibole phenocrysts in comparison to other system in the Lesser Antilles also provides a maximum reservoir depth of 8.5 Km.

Glass studies by Pichavant et al. (2018) (MI) and Metcalfe et al. (2021) (GM) allow quantification of a range of temperatures for the system. The existing reservoir, hypothesised as an andesite body (Pichavant et al., 2018), is between 825 – 875^{o}C. The recharging basalt was between 900–1025^{o}C (Metcalfe et al., 2021**)** as it intruded into the system, and hybrid magmas, as observed in the 1530 Cal. CE eruption, are 925 - 950^{o}C.

The Monts Caraïbes include the least evolved magmas observed on Basse-Terre and are often hypothesised as the parental magma from which other magmas on the island evolved, making it important to link the Monts Caraïbes to the La Soufrière magmas. The Monts Caraïbes is a large volcanic complex which began with submarine activity until the final phases which transitioned to sub-ariel Plinan activity. Eruptive activity also produced an evolved dacitic composition as well as the basaltic component studied here (Bissainte, 1995; Komorowski et al., 2005).

3 Methods

Details on the sampling areas and methods used are available in Legendre, 2012, Metcalfe et al. 2021 and in the Supplementary Material provided. Juvenile clasts were collected from both proximal and distal locations from around the vent depending on where the freshest material was available from. Detailed sample descriptions, powder, mineral and melt inclusion preparation and analysis techniques can be found the Supplementary Material.

ICP-MS was conducted on whole rock samples to measure major element concentrations. Following sieving of the samples, juvenile pyroxene and plagioclase crystals were hand separated from the 500 μm sieved fraction and analysed at the mineral core and the rim. Melt inclusions are abundant in both pyroxene and plagioclase and are observed in all samples (Fig 2). For both pyroxene and plagioclase, the selected MIs had no evidence of

leakage or post-entrapment crystallisation (PEC) and were randomly distributed through the crystal. We also favoured crystals which hosted bubble-free inclusions in order to minimise the effect of volatile loss, especially CO_2 and S, to the vapour (e.g., Venugopal et al. 2020; Table S1). Further verifications were also carried out to ensure the MI can be interpreted as the original melt composition. We also observe Na-loss from both the MI and GM, despite analysing Na first.

EMPA was conducted on minerals and glass. Major and volatile compositions were obtained for 81 polished MIs, 35 hosted in pyroxene and 46 hosted in plagioclase across the different eruptions. SIMS analysis was conducted on 33 MIs to measure H_2O, CO_2, S, Cl and F concentrations. Calibration curves were established using data ranging from basaltic-andesite to rhyolite in composition (See supplementary material; Fig S1). Deuterium (D), expressed as D/H isotope ratio, was also measured in 28 representative MIs to assess the degree of H+ diffusion which is used as a proxy for H_2O loss (See supplementary material; Fig S2).

EMPA and SIMS analyses for S, Cl and F were compared and show a good agreement for S and Cl in particular. For example, for inclusion 1101viA-pyx-5 SIMS analysis 251 ppm S and 1882 ppm Cl, in comparison EMPA analysis yielded 254 ppm S and 1720 ppm Cl. For F, however, there appears to have been some loss during EMPA analysis, for 1101viA-pyx-5 SIMS analysis yielded 433 ppm F and EMPA analysis yielded 105 ppm F.

This difference in F may be due to the higher detection limit during EMPA analyses and the overlap of the the FKα peak by the FeLα peak in these relatively Fe-rich glasses (Todd 1996; Lowenstern, 1994; Witter and Kuehner 2004**)**. For this reason, we use only the SIMS data for F.

4 Results

4.1 Whole Rock

Across Basse-Terre, bulk rock compositions from the various suites vary from basalt to dacite, with the least evolved compositions observed in the Monts Caraïbes suite in Southern Basse-Terre (Bissainte 1995; Boudon et al, 2008; Samper et al 2009; Fig 3). La Soufrière shows a narrower magma compositional range, from basalt to andesite (Boudon et al, 2008; Samper et al 2009).

This study provides further evidence that the Monts Caraïbes suite include the least evolved compositions observed on Basse-Terre showing a basaltic composition ranging from 47.6 to 48.8 wt% SiO_2 for a range of eruption products including lava and scoria (Table S2; Fig 3). The younger La Soufrière magma suite from the 1657, 1010 and 1530 Cal. CE eruptions, show a basaltic-andesite to andesite composition (55.7 to 63.9 wt% SiO_2; Fig 3), and so are more evolved than the older Monts Caraïbes magmas. Within the La Soufrière magmas, there is no clear compositional evolution with more evolved magma observed in 1530 Cal. CE (55.7 – 61.2 wt% SiO_2) and 1010 Cal. CE (60.8 - 63.9 wt% SiO_2) in comparison to the younger 1657 Cal. CE (57.9 – 62.1 wt%) samples.

The well-studied 1530 Cal. CE eruption has characteristic banding consistently observed in juvenile material with light bands are reported as ~60 wt% SiO_2 and less evolved dark bands with ~56 wt% SiO_2 (Fig 3; Boudon et al., 2008; Pichavant et al., 2018). Though the 1530 Cal. CE eruption shows a bimodal magma composition, the 1657 Cal. CE, 1010 Cal. CE and 5680 Cal. BCE eruptions appear homogeneous with no compositionally banded material observed and relatively continuous whole rock compositions.

4.2 Groundmass Texture and Composition

The groundmass textures are summarised in Table 1**.** The 1657 Cal. CE, 1010 Cal. CE and 5680 Cal. CE GM are compositionally homogenous with differences observed in the microlite content (Fig 2). The 1530 Cal. CE GM is described by Pichavant et al. (2018), Boudon et al. (2008) and Martel et al. (2021) and varies between the light and dark layers of the banded pumices.

The GM compositions are more evolved than the whole rock compositions and fall in a relatively wide compositional range from andesite to rhyolite (Table S3; Fig 3). The older eruption (5680 Cal. BCE) extends to less evolved compositions: 61.1–75.8 wt% SiO_2, 0.1– 3.6 wt% MgO, 12.5 – 22.9 wt% Al_2O_3, 1.7 – 9.7 wt% $FeO_{(total)}$, 3.1 – 8.9 wt% CaO and 0.6 – 1.9 wt% K_2O (Fig 4). In comparison, the younger eruptions (1010, 1530 and 1657 Cal. CE) show more evolved compositions: 60.6–76.3 wt% SiO_2, 0.4– 4.7 wt% MgO, 11.5 – 18.4 wt% Al_2O_3, 2.7 – 11.7 wt% $FeO_{(total)}$, 2.1 – 7.4 wt% CaO, and 0.6 – 2.3 wt% K_2O (Fig 4). Though there is a considerable overlap, the variations may relate to the abundance of microlites observed in the 5680 Cal. BCE eruption glass and not in the 1010 Cal. CE and 1657 Cal. CE.

We also observe a bimodal distribution in SiO_2 content for the 1657 CE eruption, with a high SiO_2 endmember (69.6 – 72.6 wt% SiO_2) and a low SiO_2 endmember (60.6 – 67.6 wt% SiO_2; Fig S3).

4.3 Mineral Texture and Composition

The main mineral phases in all eruptions are plagioclase and pyroxene. The majority of pyroxene are orthopyroxene with small clinopyroxene populations observed in 5680 Cal. BCE and 1657 Cal. CE. Metcalfe et al. (2021), defines six different types of orthopyroxene in different eruptions of La Soufrière based on crystal textures and zoning patterns. MI are observed in all populations with no differences observed in the MI for different crystal types.

These populations, described in full in Metcalfe et al. (2021), include three simple crystals distinguished by their zoning patterns (Type-1: one sharp compositional zone; Type-2: one diffuse compositional zone; Type-3: multiple compositional zones), two complex crystals with resorption features (Type-4: resorption rims with remaining crystal core; Type-5: completely resorbed crystals) and unzoned crystals (Type-6: no compositional zones or variations). These six populations are also identified in this study and melt inclusions are observed in all six crystal types. Orthopyroxene compositions display a narrow

compositional range, particularly within the Type-1, 2, 3 and 6 crystals (En_{55-62}). The type-4 crystal cores also fall into this narrow compositional range, while the resorbed rims fall into a different compositional range which is the same as the type-5 resorbed crystals (En_{62-67}).

The composition of pyroxene from the 1530 Cal. CE eruption is En_{56-59}, which falls in the same compositional range observed for this study (Semet et al., 1981; Poussineau, 2005; Pichavant et al., 2018). Pichavant et al. (2018) also identify a small, sporadic population of Mg-rich orthopyroxene up to En_{71}, which are closer to the resorbed compositions of type-4 and type-5 crystals in this study. Bourgeoisat (2018) splits the 1530 Cal. CE orthopyroxene into three groups based on composition related to magmatic environment (ME): ME1 (En_{56-59}), ME2 (En_{60-63}), ME3 ($En_{69-72)}$. These compositions cover the range reported for this study with ME1 and ME2 compositions covering the range observed in the simple crystal Type-1, 2, 3, 6 and 4 (cores) and ME3 are similar to the compositional range observed for Type-4 (rims) and 5.

Plagioclase is present in all the eruptions discussed and the textures observed appear consistent through the eruptions. The plagioclase crystals are tabular and euhedral to subhedral in shape. Plagioclase often has oscillatory zoning and patchy zoning in the cores (Vance, 1965). Overall, the main populations in each eruption are approximately An_{60} Ab_{40}. Additional minor populations with different compositions are observed, notably an albite-rich population (An_{20-30} Ab_{49-54}) and a very anorthite-rich population (An_{80-94} Ab_{6-19}).

For the 1530 Cal. CE eruption, narrower plagioclase compositions are reported by Pichavant et al. (2018), with a main An_{60-65} population. Anorthite-rich layers are also reported with An_{85-90} (Semet et al., 1981; Pichavant et al., 2018). This suggests that the small populations of very anorthite-rich compositions observed in the eruptions from this study may correspond to the anorthite-rich layers reported by Semet et al. (1981) and Pichavant et al. (2018).

4.4 Melt Inclusions

4.4.1 Post Entrapment Modifications

Melt inclusions are droplets of silicate and form as melt surrounding a growing crystal becomes trapped in irregularities (Sorby, 1858; Cannatelli et al., 2016; Fig 4.2). Melt inclusions are composed of glass, dissolved volatiles, vapour bubbles and crystals in variable amounts and behave as a closed system once they have become trapped in the host crystal, so theoretically retain the melts original composition. A melt inclusion is After a melt inclusion (MI) has been trapped in a host crystal it may continue to evolve independent of the melt outside of the crystal (Roedder, 1984; Bodnar et al., 1989; Steele-Macinnis, 2011). The continued evolution of the MI means the composition no longer represents the composition of the melt which was trapped. For example, crystallisation of daughter minerals or along the MI wall and diffusive re-equilibration between the MI and host crystal can all result in compositional changes (Gaetani and Watson, 2000; Schiano, 2003; Wallace, 2005; Steele-Macinnis et al., 2011). Volatiles, including CO_2 which have a

low solubility in the melt, can be lost in significant percentages to vapour bubbles (Anderson and Brown 1993; Venugopal et al., 2020).

H_2O loss from the MI can occur if the host crystal fractures or due to H^+ diffusion through the host crystal (Anderson, 1974a; Hauri, 2002; Danyushevsky et al., 2002; Wallace, 2005). The possibility of H_2O loss makes it is necessary to assess if observed H_2O trends are the result of trapping of variably degassed melts or due to H^+ loss. To assess H+ diffusion the D/H isotopic ratio can be measured, this is expressed as δD (the permil deviation from Standard Mean Ocean Water, δD_{SMOW}). For slab fluids associated to the average upper MORB mantle, δD typically falls in the range of -20 to -80 ‰ (Shaw et al., 2008). Loss of H^+ and addition of seawater and/or secondary hydrothermal fluids is also shown by positive δD values and negative correlations with H_2O (wt%) (Kyser and O'Neil, 1984; Shaw et al., 2008; Portnyagin et al., 2008). Post-entrapment modifications (PEM) can also be assessed by looking at the equilibrium between the MI and host crystals (Putirka, 2008). If the host crystal and MI are in equilibrium it can be assumed that the MI has experienced minimal post-entrapment processes such as diffusive loss and crystallisation and is representative of the original magma composition.

This included examining H^+ loss, for the eruptions discussed here, minimal H^+ loss is observed for most inclusions Generally, most inclusions fall into the D/H isotopic ratio range, expressed as δD -25 to -70‰ (Fig S2). One very positive value suggesting H^+ loss is observed for 1657 Cal. CE and one very negative value is also observed for 5680 Cal. BCE, which is due to the inclusions in this sample being small. However, as most inclusions are in the range for typical slab fluids (-20 to -80 ‰; Shaw et al., 2008), we assume the H_2O contents are representative of the magma.

Post-entrapment modification of the melt inclusions, especially the host mineral crystallisation at the walls of the MI, was assessed in two ways: (1) the MI compositions were compared to groundmass glasses and whole rock compositions in order to identify anomalous compositions with respect to the La Soufrière liquid line of descent. Though some Na_2O loss during analysis is observed, MI fit into the liquid line of descent (Fig 3 and 4). (2) Using the method of Putirka, 2008, the MI-host crystal equilibrium (K_D) was assessed and only MI in equilibrium are included in the final data set**.** For pyroxene hosted MIs and host crystal pairs the K_D is calculated by comparing the Mg/Fe ratios in the MI and host crystal (Putirka, 2008). This was also used for groundmass glass and pyroxene crystal pairs (Metcalfe et al. 2021).
MI with a K_D in the range 0.23 – 0.35 (Putirka, 2008) are considered to be in equilibrium and can be used in the dataset. The equilibrium values calculated for the pyroxene MI fall into the 0.23 – 0.35 range, with any inclusions falling outside this range excluded from the dataset (Table 2).

For plagioclase hosted MIs and host crystal pairs the K_D is calculated by comparing the albite (Ab) and anorthite (An) content of the host crystal with the Al, Ca, Na and Si content of the MI (Putirka, 2008**)**. For plagioclase the equilibrium values are temperature dependent: MI

trapped at <1050°C are in equilibrium in the range 0.05 – 0.15, and MI trapped at >1050°C are in equilibrium in the range 0.17-0.39 (Putirka, 2008). The majority of plagioclase MI record temperatures of <1050°C and K_D in the range 0.05 – 0.15. MI outside of this range were excluded from the study. The few MI recording temperatures >1050°C have K_D in the range 0.17-0.39 (Table 2).

By only including MI in the equilibrium ranges ensures all MI discussed in this paper have experienced minimal post-entrapment modifications. This includes the 1530 CE MI which are described by Pichavant et al. (2018) as having experienced no significant post-entrapment modification (See Supplementary Fig S4).

4.4.2 Major and Volatile Elements

The pyroxene MI are found across a range of crystal types described in Metcalfe et al., 2021 (Table S1). MIs of the 1657 and 1010 Cal. CE eruptions are all found in the cores and rims of simple orthopyroxene crystals (Type 1-3 and 6), while the MIs of the 5680 Cal. BCE eruption are found in cores and rims of both simple and complex orthopyroxene crystals. However, no difference in MI composition is observed between the difference crystal types.

MIs of the 5680 Cal. BCE eruption are dacitic in composition (64.6 - 76.7wt% SiO_2; see supplementary Fig S5). The majority of the MIs of the 1010 Cal. CE eruption (64.3 - 77.5 wt% SiO_2; see supplementary Fig S6) and 1657 Cal. CE eruption (73.1 – 78.2 wt% SiO_2; see supplementary Fig S6) are also dacitic in composition with few MIs of rhyolitic in composition (Fig 4; Table 2**)**. The majority MIs of the 1530 Cal. CE eruption are reported to be rhyolitic in composition with a small population which are dacitic in composition (70.5-78.7 wt% SiO_2; see supplementary Fig S6) (Poussineau, 2005; Boudon et al., 2008; Pichavant et al., 2018). There is a relatively large compositional range, however, this remains relatively constant across the eruptions studied: 64.3– 78.7 wt% SiO_2, 0.02– 2.8 wt% MgO, 11.9 – 21.3 wt% Al_2O_3, 0.6 – 8.2 wt% $FeO_{(total)}$, 1.1 – 7.0 wt% CaO, 0.05 – 4.7 wt% Na_2O and 0.7 – 2.7 wt% K_2O (Fig 4; Table 2).

For all the eruptions, with increasing SiO_2 contents CaO, FeO, MgO, MnO, Al_2O_3, TiO_2 and Na_2O decrease and K_2O increases. MIs, along with the groundmass glass, exhibit linear trends (Fig. 4; Table 2). The compositions of the MIs also show considerable overlap with the groundmass compositions. For the 1010 Cal. CE and 5680 Cal. BCE eruptions most MI are more evolved than the groundmass glass compositions, in comparison the 1657 Cal. CE eruption where MI are generally the same composition or less evolved than groundmass glass. The MIs of the 1530 Cal. CE eruption and groundmass glass compositions are very similar, with inclusions varying between being more and less evolved than glass compositions (Boudon et al., 2008, Poussineau, 2005; Pichavant et al., 2018).

We also observe variations that distinguish between the VEI 4 eruptions and the VEI 2-3 eruptions when looking at the average MI SiO_2. The average MI SiO_2 (wt%) is lower for both the VEI 4 eruptions (1010 CE – 71.6 wt% SiO_2, 5680 BCE – 72.7 wt% SiO_2) in comparison to

the VEI 2-3 eruptions (1657 CE – 76.1 wt% SiO_2 and 1010 CE – 74.3 wt% SiO_2). Giving a compositional gap of 1.6 - 4.5 wt% SiO_2 between the two VEI 4 and VEI 2-3 eruptions.

The range of water across the eruptions is 1.3 - 4.4 wt%, with little variation in the water content between eruptions (5680 Cal. BCE: 2.4 - 4.2 wt%; 1010 Cal. CE: 1.3 - 4.4 wt% and 1657 Cal. CE: 2.3 - 4.1 wt% (Fig 5A; Table 2)). The reported range for the 1530 Cal. CE eruption is 2.5 - 5.6 wt% H_2O, however, most inclusions are reported to have 5 - 5.5 wt% H_2O which is higher than recorded for the eruptions in this study (Pichavant et al., 2018) (Fig 5A; Table 2).

In comparison to H_2O contents, CO_2 contents vary greatly across the eruptions. The range measured in bubble-free MI across the eruptions is 11 – 866 ppm. The highest CO_2 contents are recorded for the 5680 Cal. CE eruption with a range from 116-866 ppm. The lowest CO_2 contents are recorded for the 1010 Cal. CE eruption with CO_2 contents often below the detection limit and a range from 11 – 405 ppm. The CO_2 contents for the 1657 Cal. CE eruption ranges from 35 - 674 ppm. Across the eruptions CO_2 contents decrease with increasing K_2O (Fig 5B; Table 2). No CO_2 contents have been published for 1530 Cal. CE.

Sulphur (S) is relatively consistent across the eruptions, ranging from 20-777 ppm. There is little difference S content between the eruptions (e.g., 5680 Cal. BCE: 20-777 ppm; 1010 Cal. CE: 57-654 ppm and 1657 Cal. CE: 30-564 ppm. The S contents reported for 1530 Cal. CE (184-495 ppm) by Poussineau (2005) and Pichavant et al. (2018) also fall in this range (Fig 5C; Table 2).

Chlorine (Cl) has a range of 892 - 3610 ppm across the eruptions. Similar to S, there is little variation in the Cl content between eruptions (e.g., 5680 Cal. BCE: 1041 – 2551 ppm; 1010 Cal. CE: 1458-3198 ppm and 1657 Cal. CE: 892 – 3610 ppm (Fig 5D; Table 2). The Cl contents reported for 1530 Cal. CE (2462- 3006 ppm) by Poussineau, 2005 and Pichavant et al., 2018 also fall in this range.

Fluorine (F) content ranges from 350 to 610 ppm across the eruptions (only SIMS data). The F data shows little variation between eruptions (5680 Cal. BCE: 370 - 610 ppm; 1010 Cal. CE: 350 - 483 ppm and 1657 Cal. CE: 400-510 ppm (Fig 5E; Table 2)). No F contents have been published for 1530 Cal. CE.

The total volatile content across the eruptions is relatively consistent with the majority of the total volatiles made up by H_2O (Fig 5F; Table 2): 5680 Cal. BCE - 4.7 wt%; 1010 Cal. CE - 5.1 wt%; 1530 Cal. CE - 5.3 wt%; 1657 Cal. CE - 4.7 wt%.

5 Discussion

5.1 The Mush Model of La Soufrière

5.1.1 Magmatic Conditions

The results of our MI analysis allow us to incorporate a more accurate understanding of temperatures, pressures, depths and melt compositions into the mush model proposed by

Metcalfe et al. (2021) for La Soufrière. Scandone et al. (2007) schematise four regions to describe the generation and ascent of magma in a general context: (i) the deepest part of the system: the supply system, (ii) the intermediate storage: the mush zone, (iii) the conduit, (iv) the vent. The four regions are not necessarily simultaneously connected depending on the supply rate from the supply system and processes occurring in the mush storage zone. Here we use a similar schematic and our study focuses on the mush storage zone. This region is formed from repeated intrusions from the supply system and is composed of an interlocking framework of crystals which melt is distributed through the mush in varying volumetric proportions. Melt and/or fluid migration, amalgamation and mixing make the system inherently unstable allowing remobilisation for example, by pressure increase from crystallisation or influxes of new magma (Scandone et al., 2007; Costa et al., 2009; Mader et al., 2013; Moretti et al., 2013; Brown et al., 2014; Rubin et al., 2017; Cooper and Kent, 2014; Sparks and Cashman, 2017; Jackson et al 2018).

The MIs show that the composition of the La Soufrière magma has remained relatively stable across the eruptions studied here, and no compositional evolution across the history of the system is observed (Fig 4). This suggests that the composition of any new magma inputs has also remained relatively similar. However, as the MI from the La Soufrière eruptions show an evolved composition, these MI do not preserve the primitive melt composition feeding this system. Based on this, we can only make inferences about the mush storage region and not on deeper processes occurring in the supply zone involving more primitive melts.

The MI and GM relationship provides further evidence of a mush storage zone at La Soufrière (Fig 4). The fact that some MI have a more evolved composition than the GM indicates the MI have cooled prior to interaction with the GM and are exotic to the transporting melt (e.g., Kilgour et al., 2013). This is possible if the transporting melt entrains MI-bearing crystals stored in the mush system. The 5680 Cal. BCE, 1010 Cal. CE, 1530 Cal. CE and 1657 Cal. CE eruptions all have MI which are more evolved than the GM glass, indicating MIs have been entrained from the mush lenses in the erupting melt. This could be particularly important for the 5680 Cal. BCE eruption where orthopyroxene crystals are observed to have resorption rims (Metcalfe et al., 2021).

The MIs can also be used to calculate the properties of the mush storage zone. The thermobarometers of Putirka (2008) were used to calculate the temperatures for both MI (Putirka, 2008 eq. 24a for plagioclase, eq. 28a for orthopyroxene and eq. 33 for clinopyroxene) and groundmass glass (with orthopyroxene rims, Putirka, 2008: eq. 28a; Metcalfe et al. 2021), this thermobarometer has an error of ±30^{o}C. For each eruption, MI record a range of temperatures: 965 – 1110^{o}C for 5680 Cal. BCE, 960 – 1050^{o}C for 1010 Cal. CE, and 945 – 1050^{o}C for 1657 Cal. CE (Fig 6A). GM record a range of temperatures: 870 – 1085^{o}C for 5680 Cal. BCE, 1010 – 1025^{o}C for 1010 Cal. CE, and 950 – 1020^{o}C for 1657 Cal. CE (Fig 6A). The temperatures reported by Pichavant et al., (2018) for 1530 Cal. CE (825-1025^{o}C) are in a similar range as those calculated for this study. (Fig 6A). For the 1657 CE,

1010 CE and 5680 BCE eruptions there is significant overlap between the mean MI (1000 ±SD 40 °C, 1000 ±SD 35 °C and 1020 ±SD 36 °C, respectively) and GM temperatures (975 ±SD 24 °C, 980 ±SD 8 °C and 990 ±SD 72 °C, respectively).

Using the method of Papale et al. (2006) minimum pressures were calculated using the highest H_2O and CO_2 contents recorded by MIs for each eruption. The ferric and ferrous iron con- tents of the melt were estimated using Kress and Carmichael (1991) which is integrated into Magmasat (Ghiorso and Gualda, 2015). This shows the pressure of MI entrapment ranges from 190 MPa to 220 MPa (Fig 6B). These pressures are similar to the pressure of 170 MPa reported by Pichavant et al. (2018) for the 1530 Cal. CE eruption (Fig 6B). Converting the pressures to depths using a density of 2450 kg m^{-3} (Barnoud et al., 2016) indicates that these eruptions at La Soufrière were fed by melts originating from minimum depths of ~7 to 9 km within the mush storage zone. However, different eruptions were fed by melt originating from different areas of the mush storage zone and the 5680 Cal. BCE eruption was fed from the deepest source at ~8.7 Km. This shows the eruptions of La Soufrière studied here have been fed from a narrow range of depths within the mush system.

Oxygen fugacity (fO_2) affects magma phase equilibria, density and rheology because of redox reactions affecting fluid speciation and iron speciation in melts (Kress and Carmichael, 1991; Campbell et al., 2009; Moretti and Papale, 2004; Burgisser and Scaillet, 2007; Moretti and Stefansson, 2020). In this study, we adopt the Kress and Carmichael (1991) equation, which is included in the Ghiorso and Sack (1995) model for natural magmas' phase equilibria. This allows fO_2 to be defined from a measured melt composition and calculated temperature and pressure. For La Soufrière, this model shows the logfO_2 ranges from -9.1 - -9.4. For each eruption the average ΔNNO values are: +0.86 (5680 Cal. BCE), +0.79 (1010 Cal. CE) and +0.85 (1657 Cal. CE), calculated using the average melt inclusion temperatures (1020°C, 1000°C and 1000°C, respectively). These values are in the same range reported for 1530 Cal CE (ΔNNO+0.8) by Pichavant et al. (2018) and indicates that the fO_2 of melts at La Soufrière has remained relatively constant through time.

5.1.2 Magmatic Processes at Depth

Understanding the processes occurring in the storage zone is important to understand the dynamics, chronology and style of eruptions. Pichavant et al. (2018) use melt inclusions and experimental data to investigate the processes driving the 1530 Cal. CE eruption. For this eruption, the andesite in the storage zone is remobilised by the arrival of a less evolved basaltic magma. Mixing between the andesite and basalt forms a hybrid magma where banded material is extracted from. The mixing is incomplete with an unmixed andesite, hybrid magma and unmixed basalt present. In this scenario, recharge by a less evolved magma from depth is needed to explain the observed eruption products and compositions.

The eruptions detailed in the present work, in contrast to 1530 Cal. CE, do not show any textural evidence of mixing with more primitive compositions which may have triggered the

eruption. However, for the 1657 CE eruption there is some evidence for a bimodal distribution within the groundmass glass compositions which could indicate incomplete mixing of high and low SiO_2 melts (Fig S3). This suggests both the 1657 Cal. CE and 1530 Cal. CE eruptions may have been driven by mafic recharge intruding into the storage zone.

For the 1010 Cal. CE and 5680 Cal. BCE eruptions, the lack of compositional and textural evidence for mixing could indicate that recharges from the supply system have not been involved in these eruptions. Alternatively, efficient mixing could have occurred, or magmas preserving mixing textures have not been erupted. In this case, mafic recharge would prompt the reactivation of shallow magmas by supplying it with fluids and heat, as for other volcanoes of Lesser Antilles (e.g., Edmonds et al., 2010; Solaro et al., 2020).

Furthermore, the occurrence of potential mafic recharge may explain the lack of compositional evolution across the samples, with the compositions related to the volumes of mafic/evolved endmembers and the efficiency of magma mixing. Alternatively, the fact that not all parts of the mush system may be tapped during eruption would again contribute to the lack of any broad compositional evolution (Metcalfe et al., 2021).

The compositional gap between the VEI 4 eruptions and the VEI 2-3 eruptions could suggest the Plinian events erupted well-mixed, moderately evolved magmas. In comparison, the lower magnitude eruptions erupted poorly mixed magmas with the MI representing the mush-zone magma and evidence for mixing observed in groundmass glass compositions and textures. Poorly mixed magmas are widely recorded for VEI 2-3 eruptions at arc volcanoes, including: Turrialba (DeVitre et al., 2019); Santiaguito (Wallace et al., 2020); Tungurahua (Myers et al., 2014); Mt Unzen (Nakamura, 1995); Kasatochi (Neill et al., 2015); Soufriere Hills, Montserrat (Barclay et al., 2010; Edmonds et al., 2010) and Kelud (Jeffery et al., 2013).

We also consider the possibility that a more evolved melt migrated through the mush zone following the 1010 CE eruption, and that subsequent mafic injections interacted and began to mix and mingle with the more evolved melt to produce to 1530 CE (very poorly mixed) and 1657 CE (moderately poorly mixed) eruption products.

5.2 Controls on Eruption Style

The overall stability of the temperature and depth (7 - 9 Km) indicates the storage zone has remained relatively stable over time. Though the eruptions studied here have been fed from a relatively narrow range of depths, we cannot rule out that the mush system may extend over a larger range of depths. Although the composition and volume of any potential mafic recharge may also result in variation in eruption style, this suggests that factors and processes occurring above the magma storage zone and within the conduit system may also play a considerable role in controlling eruption style. These processes include degassing of the ascending magmas, rheological changes and the interactions with other top-down processes of non-magmatic but external origin. Particularly in a mushy system, these processes modulate to various extents the magma ascent rate, which initially is ideally

imposed by the mass flux at the exit of the magma storage zone. Therefore, though eruption style may be determined by factors and processes occurring above the magma storage zone, and not influenced by dynamics in the magma storage zone, the magma storage zone must still be considered to play a role in driving the build-up to an eruption.

5.2.1 Volatiles

Volatiles are considered to be an important control on eruption style (Blundy and Cashman, 2005; Dingwell, 1996; Melnik and Sparks, 2002). Volatiles, in particular H_2O, have an important control on magma ascent. Degassing during ascent leads to degassing-induced crystallisation (Cashman and Blundy, 2000; Cashman, 2004) which promotes further volatile exsolution and results in changes in magma rheology (Dingwell, 1996; Edmonds and Wallace, 2017). Alternatively, exsolution-driven volatile expansion drives fast ascent which results in high volatile overpressure in bubbles and high strain rates from rapid acceleration leading to explosive fragmentation (Roggensack et al., 1997; Papale, 1999; Huppert and Woods, 2002; Scaillet et al., 2008; Owen et al., 2013; Cassidy et al., 2016; Bernard and Bouvet de Maisonneuve, 2020).

In the case of La Soufrière, it could be expected that the large magnitude eruptions of Plinian style were driven by higher H_2O contents. However, no discernible differences are observed, with the large 5680 Cal. BCE and 1010 Cal. CE Plinian eruptions and the 1657 Cal. CE Vulcanian eruption having <0.3 wt% difference in H_2O content.

Open system degassing and fluxing of CO_2 are important process at some systems to drive explosive eruptions (Sable et al., 2006; Aiuppa et al., 2011; Blundy et al., 2010; Moretti et al., 2019; Assbichler, 2020; Allison et al., 2021). However, the plot of H_2O versus CO_2 shows no clear degassing trends, instead the wide spread of H_2O and CO_2 contents indicates complex degassing histories and the trapping of variably degassied melt (Schmitt 2001; Atlas et al. 2006; Johnson et al. 2010; Blundy et al. 2010; Reubi et al., 2013; Fig S8).

The fluxing of CO_2 occurs because deep melts with high CO_2 contents degas and supply CO_2 to shallow ascending magmas but it seems to control the eruption style wherever the total (exsolved + dissolved) CO_2 amount is high (>0.6. wt%, Allison et al., 2021; > 1.5 wt% in most cases, Blundy et al., 2010; Moretti et al., 2018, 2019). Current data do not allow total CO_2 in the system to be assessed reliably (e.g., Barsanti et al., 2009; Moretti et al., 2018), but based on degassing and fluxing simulations carried out on Montserrat volcanoes total CO_2 is not expected to be larger than 0.2 wt%, inferred from the amount dissolved in the unerupted underplating basalt (Edmonds et al., 2010). Considering that CO_2 contents measured in this study for La Soufrière are even lower (<0.1 wt%), which is also the case for Montserrat basalt values, we can conclude the total CO_2 content is not a major control, with H_2O making up the majority of the total volatile content.

Assuming that the bulk dissolved content of the most primitive MIs approximate the total volatile content of magmas in their subsequent evolution toward pre-eruptive conditions, there is <1 wt% difference in total volatile content across the eruptions studied, suggesting

660 the volatile content cannot be the main controlling parameter for eruption style (Fig 5F).
661 Comparing the total volatile content against VEI highlights that, for these eruptions, volatile
662 content does not control explosivity (Fig 5F). However, we cannot discount the effect of an
663 exsolved fluid phase on the eruption style. At La Soufrière, gas measurements currently
664 acquired over the active fumarolic field allow to quantify the degassing volatile flux.
665 However, the lack of such data for past eruptions to compare with our MI dataset
666 significantly complicates the understanding of the exsolved fluid phase. Further to this,
667 current measurements of the gas phase composition at the surface do not reproduce the
668 pre-eruptive magmatic volatile phase at depth because the well-developed hydrothermal
669 system scrubs the magmatic signal (Symonds et al., 2001; Moretti et al., 2020; Moune et al.,
670 2022).

671 **5.2.2 Viscosity Changes**

672 To investigate how the magma has changed during ascent and eruption we investigate the
673 syn-eruptive change of flow behavior. Crystallization in the conduit can abruptly modify
674 magma properties and effect eruption style (Gardner et al., 1998; Nakada et al., 1999;
675 D'Oriano et al., 2005; Di Genova et al., 2017; Hlinka, 2020; Romano et al., 2020; Vona et al.,
676 2020; Hlinka et al., 2021). As the MI are trapped in phenocrysts formed in the storage zone,
677 we instead use GM viscosity where the microlite crystallization relates to changes occurring
678 in the conduit during magma ascent prior eruption (Hlinka, 2020; Hlinka et al., 2021). We
679 assume crystallization of the GM occurred in the conduit and was quenched on eruption
680 and no further crystallization occurred after eruption.

681 The syn-eruptive crystal fraction in the GM varies for each eruption (Table 3), with the
682 largest variation observed between the 5680 Cal. BCE microlite-rich Plinian eruption and the
683 1010 Cal. CE microlite-poor Plinian eruption. The ConFlow 1.0.5 model (Mastin, 2002) is
684 used to calculate the groundmass viscosity as this model takes into consideration
685 crystallinity. Using the ConFlow 1.0.5 model (Mastin, 2002) crystal-free viscosity model,
686 mean glass composition, magma temperature and pressure we calculate GM viscosities
687 ranging from $10^{5.4}$ Pa·s to $10^{8.2}$ Pa·s (Table 3; Fig 6C). Notably, the two Plinian eruptions
688 (5680 Cal. BCE and 1010 Cal. CE) are characterised by lower viscosities than the two
689 smaller eruptions (1530 Cal. CE and 1657 Cal. CE) (Fig 6C). This is one of the only
690 properties which shows a clear difference between the more explosive (VEI 4) and less
691 explosive (VEI 2-3) eruptions.

692 Using the microlite vol%, mean glass composition and the ConFlow 1.0.5 model (Mastin,
693 2002) we calculate the melt viscosity after syn-eruptive crystallisation (GM+X) (Figure 6C).
694 The resulting increase in the effective viscosity between GM and GM+X indicates an
695 increase in potential for explosivity for the 1657 Cal. CE, 1530 Cal. CE and particularly, the
696 5680 Cal. BCE eruptions (e.g., Houghton and Gonnermann, 2008; Moitra et al., 2018; Arzilli
697 et al., 2019; Hlinka, 2020; Hlinka et al., 2021). The range of viscosities calculated for La
698 Soufrière have a similar range to viscosities calculated in the literature (See Supplementary
699 Fig S9), which for groundmass glass without microlites range from $10^{1.9}$ - $10^{8.2}$ Pa·s and for

groundmass glass with microlites range from $10^2 – 10^{9.7}$ Pa·s (Taddeucci, et al., 2004; Lautze and Houghton, 2007; Pappalardo et al., 2018; Mujin and Nakamura, 2020; Hlinka et al., 2021).

The 5680 Cal. BCE eruption experienced a larger viscosity increase than the 1657 and 1530 Cal. CE eruptions, suggesting the magma feeding the 5680 Cal. BCE eruption had a higher explosivity following ascent. This large viscosity change may have resulted in the 5680 Cal. BCE eruption being the largest Plinian eruption in the La Soufrière record. However, viscosity changes cannot be the only cause of Plinian eruptions at this system, as a large viscosity change is not observed for the magma feeding the 1010 Cal. CE Plinian eruption. For the 1010 Cal. CE eruption a combination of other factors may result in the culmination of a Plinian eruption.

5.2.3 Ascent Rate

The ascent rate is the rate which magma ascends through the conduit from the magma mush storage zone to the surface and is a function of pressure magma density, viscosity, and resistance to flow while in the conduit (Papale and Dobran 1994; Mastin and Ghiorso 2001; Pinkerton et al. 2002; Sparks et al. 2006; Rutherford, 2008). Ascent rate has been shown to be an important factor in controlling the onset of fragmentation, hence the transition between eruption styles and so may also be a key parameter to explain the differences in eruption styles observed at La Soufrière (e.g., Cassidy et al., 2018).

Here we simplify magma ascent to fast and slow relative to the rates calculated. The ascents calculated refer to an average velocity from the storage system to the surface, though in reality magma ascent rate will vary through the conduit due to changes in vesicularity and volatile content, overpressure at depth, magma rheology and conduit geometry.

ConFlow 1.0.5 from Mastin (2002) is used to calculate ascent rate based on crystal volume % and mean GM composition. The model also requires the input of temperature, pressure and depth (taken from Putirka, 2008 and Papale et al., 2006 calculations). Conduit diameter is also required when using this model and is the largest unknown as no magmatic eruptions have been observed at La Soufrière so estimates must be used.

The conduit is defined as the connection between the magma storage area and the surface (Wilson et al., 1980; Bower and Woods, 1996). In explosive eruptions at more evolved systems the conduit is hypothesised to begin as a small fracture which widens allowing higher velocities, resulting in erosion of the conduit and widening into the vent (Wilson et al., 1980). To simplify the model, the conduit is assumed to be a vertical cylinder with a constant radius from the storage area to the surface which does not include any widening in the upper parts of the conduit or the vent radius (Fedotov, 1981; Colucci et al., 2014).

One way to estimate conduit diameter is to look at similar systems. At the neighbouring volcano Soufrière Hills Volcano, Montserrat, a conduit radius of 15 m has been estimated for the sub-Plinian eruption on 17th September 1996 (Robertson et al., 1998). This is based on Bower and Woods (1996) which models a sustained discharge from a narrow conduit

into a wide crater, from the initial crater dimensions, spine widths from earlier eruption phases and fluid dynamic models (Robertson et al., 1998). A 15 m radius is also estimated for smaller Vulcanian eruptions occurring at Soufrière Hills Volcano during August 1997 where a 30 m ±5 m diameter conduit, widening into a flared crater was estimated using spine dimensions, magma ascent rates and volume extrusion rates (Voight et al., 1999; Clarke et al., 2002). A radius of 15 m has also been used for modelling the dynamics of lava dome extrusion during the 1995-1999 period (Devine et al., 1998; Melnik and Sparks, 1999). Based on this we used conduit diameters of 10, 20, 30, 40 m to cover the observed conduits at Montserrat. ConFlow 1.0.5 assumes the conduit is vertical and circular in cross section.

For 10 to 40 m diameters, this model gives ascent rates of 0.7 – 3 m/s for the 1657 Cal. CE Vulcanian eruption and 2 – 4 m/s for the 1530 Cal. CE sub-Plinian eruption (using the average microlite vol% to give an average ascent rate), respectively (Figure 6D; Table 3). The two Plinian eruptions could be expected to have similar ascent rate however, the 1010 Cal. CE Plinian eruption is characterised by a fast ascent rate of 0.6 – 12 m/s in comparison the 5680 Cal. BCE Plinian eruption which is characterised by the slowest ascent rate of 0.04 -1 m/s. This difference is related to the feedback loop between ascent rate and microlite growth which leads to a slower ascent rate in the microlite-rich 5680 Cal. BCE eruption (Cassidy et al., 2018).

5.3 Top-Down, Bottom-Up and External Processes

The transition in explosive eruption style at La Soufrière is not related to any large changes in the mush storage region or supply system, as shown by the lack of compositional and volatile differences in the magmas feeding the different eruption styles. The variations in ascent rate (Fig 6D) indicate that faster ascent rates often lead to more intense eruptions, the ascent rate variations may relate to mass flux entering the conduit. However, the range in viscosity changes indicate processes occurring above the magma storage zone and within the conduit also control eruption style and explosivity. This suggests that externals factors and the interplay of top-down and bottom-up controls must be considered for the La Soufrière system.

At andesitic volcanoes such as La Soufrière, top-down controls are related to the extent and dynamics of the hydrothermal system on magma in the conduit and the presence of lava lakes as well as of caldera structures and lava domes (e.g., Endo et al., 1981; Alidibirov and Dingwell et al., 1996; Sparks, 1997; Scandone et al., 2007; Boudon et al., 2015; Cassidy et al., 2018; Heap et al., 2019). In this context, fracture-generating processes driven by thermo-hydraulic circulation, hydrothermal inflation and rock alteration result in the establishment of connectivity between the lower-pressure upper zones and the deeper pressurised regions of the plumbing system (Roman and Cashman, 2018). A lava dome can favour pressure build-up by sealing shallow outgassing fractures (Taisne and Jaupart, 2008; Boudon et al., 2015; Chevalier et al., 2017) or plugging the conduit (Diller et al., 2006; Collinson and Neuberg, 2012; Boudon et al., 2015; Bain et al., 2019). Explosions are promoted by smaller

domes where pressure build up is sufficient to overcome load pressures; as the lava dome load increases pressure build up may become insufficient to overcome the lava dome load pressure and strength (Taisne and Jaupart, 2008; Boudon et al., 2015). Lava domes can also modulate explosions during long-lived activity. If pressure builds up below a 'plugging' dome (Johnson et al., 2014), magma may fragment through tensile failure (Hornby et al., 2019) leading to explosive eruptions. Larger lava domes are also less likely to become efficiently sealed as deep-seated fractures are more likely to form in the the outer parts of the lava dome increasing the permeability (Boudon et al., 2015). Sector collapses and phreato-magmatic interactions may also greatly enhance or even trigger highly explosive activity (Pinel and Jaupart et al., 2000; Scandone et al., 2007).

La Soufrière has a history of dome emplacement, large dome collapse events, high amounts of external water and also has a well-developed and active hydrothermal system, which forms quickly at any hot cycle of volcanic activity. Hydrothermal alteration results in modifications to the shape of the pore network, this can result in reductions in permeability and porosity, decreasing volcano stability and increasing pore pressure and promoting explosive behaviour (e.g., Lopez and Williams et al., 1993; Sparks, 1997; Komorowski et al., 1997; Reid, 2004; Komorowski et al., 2010; Pola et al., 2012; Ball et al., 2013; Wyering et al., 2015; Navelot et al., 2018; Heap et al., 2019; Heap et al., 2021; Komorowski et al., in prep). Like for many andesitic volcanoes, these major features of the La Soufrière system must be considered as controlling effects on magmatic eruption style.

The influence of the hydrothermal system alteration at La Soufrière (e.g., Navelot et al., 2018) and external forcing has already been proposed as important controls on phreatic eruptions (Zlotnicki et al., 1992; Moune et al., 2022). High fluid circulation combined with sealing of the dome with pressure unable to be released increases the risk of a phreatic eruption, as hypothesised for the 1976-77 eruption (Zlotnicki et al., 1992). An alternative hypothesis proposed for the 1976-77 eruption is the efficient, extensive hydrothermal system might buffer the rise of small magma batches, leading to their stagnation at shallow depth and limiting the eruption active to only phreatic explosions (Feuillard et al., 1983; Villemant et al., 2014). It is therefore also important to understand the potential control of the hydrothermal system and external forcing on a magma ascent and its eruption potential and explosivity.

5.3.1 The 5680 Cal. BCE Plinian eruption (VEI 4) – slow ascent and the importance of top-down controls

As no temperature differences within the error estimates are observed between the average GM (990^{o}C) and MI (1035^{o}C), this could indicate that any magma moving from the supply system is not preserved in the erupted area of the storage zone. Instead, processes of mixing different parts of the same mush may be more relevant (e.g., Solaro et al., 2020). This could be considered a realistic scenario based on: the lack of GM mixing textures, homogenous MI composition in both the Type 1, 2, 3 and 6 OPX and Type-4 and 5 OPX and

MIs and GM glass show considerable compositional overlap. Alternatively, magmas may have been well mixed prior to eruption.

The final destabilisation of the mush system has affected the majority of the erupted area of the storage zone (~9 Km depth) 40 days before eruption (Metcalfe et al., 2021) (Fig 7A). In comparison, to the other eruptions discussed here, the 5680 Cal. BCE eruption had a slow ascent rate (0.04 – 1 m/s).

Prior to the 5680 Cal. BCE eruption, lava flow and dome extrusions were identified in the eruptive record (Samper et al., 2009; Legendre, 2012). This effusive period of activity followed in eruptive record directly by the explosive Plinian eruption (Legendre, 2012), with the transition of effusive to explosive activity potentially influenced by the upper conduit and vent (Sparks, 1997; Platz et al., 2007; Castro and Gardner, 2008; Cassidy et al., 2018).

This transition can be explained by the properties calculated for the 5680 Cal. BCE magma. The slow ascent observed for this eruption should have allowed volatiles to decouple from the magma under an open-system degassing regime (Gonnermann and Manga, 2013). Feedbacks between degassing and crystallization (observed in this eruption which is characterised by a high microlite content) were able to increase viscosity and slow ascent further allowing more degassing. Such gas loss would have favoured the occurrence of an effusive eruption (Melnik and Sparks, 1999; Cassidy et al., 2018) (Fig 7A).

However, the syn-eruptive viscosity changes resulting from degassing and crystallization feedbacks and the conduit sealing related to a lava dome and/or hydrothermal processes would have reduced outgassing efficiency (Sparks, 1997; Komorowski et al., 1997; 2010). With the combination of microlite growth creating large pressure gradients and gas accumulation beneath the sealed dome, leading to pressurisation of the magma (Sparks, 1997; Cassidy et al., 2015).

The pressure increase is contained by the elastic deformation of the wall rocks until this overpressure exceeds the strength of the confining rock and the seal fails resulting in this case, a Plinian eruption (Cortés et al., 1997, Barmin et al., 2002, Lavallée et al., 2012; Boudon et al., 2015). This scenario of slow ascending magmas resulting in explosive eruptions has been shown to occur at several systems including the Inyo volcanic chain, USA (Castro and Gardner, 2008).

5.3.2 The 1010 Cal. CE Plinian phase (VEI 4)– fast ascent and the importance of bottom-up controls

Similar to the 5680 Cal. BCE, no temperature differences within the error estimates are observed between the average groundmass glass (1025^{o}C) and MI (1000^{o}C) for the 1010 Cal. CE eruption. Again, this could indicate that any magma moving from the supply system did not directly impact the erupted area of the storage zone. As with 5680 Cal. BCE, mixing different parts of the same mush may have occurred (e.g., Solaro et al., 2020). This is again shown by: the lack of GM mixing textures, MIs and GM glass show considerable

compositional overlap and homogenous MI composition in the Type 1, 2, 3 and 6 OPX. Alternatively, magmas may have been well mixed prior to eruption.

The final destabilisation of the mush system has affected the majority of the erupted area of the storage zone (~9 Km depth) 848 days before eruption **(**Metcalfe et al., 2021). In comparison to the shorter diffusion timescales calculated for other eruptions, which are on the scale of days to weeks, this indicates that recharge and mixing in the storage zone has occurred over a long period. Despite the magma's long residence in the storage zone, magma has ascended relatively rapidly in the conduit (0.6 -12 m/s) in comparison to the other eruptions.

The 1010 Cal. CE explosive eruption was followed by an effusive phase (Legendre, 2012). Though the previous eruption (450 Cal. CE) was an effusive eruption, it is unclear whether prior to the 1010 Cal. CE eruption a dome was emplaced, if a dome was present our results suggest that the state of the upper conduit and vent has not had a major control on the 1010 Cal. CE eruption (Fig 7B).

Instead, volatile exsolution drove rapid ascent by increasing buoyancy, during fast ascent outgassing is less efficient with exsolved volatiles remain coupled to the melt in a closed-system degassing scenario (Mangan and Sisson, 2000; Cashman, 2004; Szramek et al., 2006). The small syn-eruptive viscosity change observed for the 1010 Cal. CE and microlite-poor groundmass indicates that decompression-induced crystallisation was limited, and has resulted in fluid-like behaviour by reducing viscosity and further increasing magma buoyancy (Anderson, 1995; Martel, 1998; Scandone et al., 2007; Massol and Jaupart, 1999; Martel, 2012). This rapid ascent of a magma with volatiles coupled to the melt in a closed system led to high overpressures and promoted explosive behaviour. Driven from the 'bottom-up' the rapid ascent of a gas-rich magma led to explosive fragmentation and a Plinian eruption (Cassidy et al., 2018; Fig 7B). A slower ascent rate, as in the case of 1657 Cal. CE may have resulted in a less explosive eruption (e.g., Szramek et al., 2006).

5.3.3 The 1530 Cal. CE Sub-Plinian phase (VEI 3) – the importance of external forces

The 1530 Cal. CE eruption began with injection of a less evolved magma from the supply system into the storage system (Pichavant et al., 2018). Magma then ascended at 2-4 m/s through the conduit, an ascent rate that is most comparable to the magma ascent rate for the 1657 Cal. CE eruption.

The microlite-poor (17 vol%) glass observed in the light bands of the banded 1530 Cal. CE eruption products, are comparable to the 1657 Cal. CE groundmass glasses (18 vol%). However, the 1530 Cal. CE has the additional homogenous glass (27 vol%) and glass from dark bands (34 vol%) that are compositionally different. This wider range of textures indicates more complex processes affected the conduit.

The 1530 Cal. CE eruption is the most well-constrained La Soufrière eruption. It began with a phreatic phase followed by a flank collapse which preceded the arrival of magma at the surface and fed the sub-Plinian explosive phase discussed throughout this paper

(Komorowski et al., 2005; 2008; Touboul et al., 2007; Boudon et al., 2008; Pichavant et al., 2018). The andesite magma was erupted first transitioning through banded black and white pumice and then to basaltic-andesite. Following the sub-Plinian phase the eruption style changed to strombolian activity and a less explosive phase, with the end of the multiphase eruption marked by the growth of the current andesite lava dome (Boudon et al., 2008).

The flank collapse prior to the sub-Plinian phase indicates that external forces have had a major control on the generation of this magmatic eruption (Boudon et al., 2003; Boudon et al., 2007). The volcanic edifice can exert a large load which affects the stress field at depth reservoir (Pinel and Jaupart, 2000, 2005). A flank collapse rapidly releases this load resulting in a downward propagating pressure change which affects the decompression rate of the magma resulting in fragmentation and in this case, contribute to the triggering of a sub-Plinian eruption style (Boudon et al., 2003; Pinel and Jaupart, 2005; Gudmundsson, 2006; Scandone et al., 2007).

The stress fields exerted by the edifice can also affect the petrological and chemical evolution of the magma in the storage zone and can prevent denser, less evolved magmas reaching the surface (Pinel and Jaupart, 2000, 2005; Gudmundsson, 2006). At several volcanoes including. Mount St. Helens (Pinel and Jaupart, 2000), Bezymianny volcano (Kamchatka, Russia) (Izbekov et al., 2006) and volcanoes in the Lesser Antilles including on Martinique and St Lucia (Boudon et al., 2013), the unloading of the volcanic edifice and change in stress field from events such as flank collapse have been shown to result in a change in magma composition to more mafic compositions erupted after the collapse event (Pinel and Jaupart, 2000). This may be a plausible scenario for the 1530 Cal. CE eruption with changes in the stress field controlling the transition from andesite to black and white banded pumice and then to basaltic-andesite which were present in the storage zone following the recharge event. In comparison, the other eruptions do not have a banded component and flank collapses were not thought to have occurred directly before a magmatic explosive eruption.

5.3.4 The 1657 Cal. CE Vulcanian eruption (VEI 2) – fast ascent and the importance of bottom-up controls

As with the two Plinian eruptions no temperature differences within the error estimates are observed between the average groundmass glass ((975^{o}C) and MI (1000^{o}C) for the 1010 Cal. CE eruption. There are also no GM mixing textures, MIs and GM glass show considerable compositional overlap and homogenous MI composition in the Type 1, 2, 3 and 6 OPX. There is also some bimodal variation in the groundmass glass compositions. This suggests mafic recharge may have occurred prior to this eruption and resulted in incomplete mixing. The final destabilisation of the mush system has affected the majority of the erupted area of the storage zone 35 days before eruption (Metcalfe et al., 2021). Eruptible magma then ascended from ~8 Km depth in the storage region into the conduit and then to the surface.

Though this eruption did not have an effusive phase, the 1530 Cal. CE dome, still present today, was emplaced prior to the 1657 Cal. CE eruption (Komorowski et al., 2005; Boudon et al., 2008; Legendre, 2012). For the 5680 cal. BCE eruption the dome and top-down controls have had a major effect on producing the explosive eruption. However, for 1657 Cal. CE the evidence for the occurrence of similar major top-down controls is not clear.

Given the composition and volatile contents of the 1010 Cal. CE and 1657 Cal. CE eruptions are very similar, the magma could have been expected to ascend in similar ways and to lead similar explosive eruptions. However, magma in the 1657 Cal. CE eruption had a slower ascent rate and experienced a larger syn-eruptive viscosity change. The slower ascent rate may have allowed more time for microlite crystallisation in the magma of the 1657 Cal. CE eruption than in the 1010 Cal. CE eruption, a process that in turn increased its viscosity (Sparks, 1997; Melnik and Sparks, 1999). The viscosity change that resulted from microlite crystallisation in a closed-system promoted some limited explosivity of the small magma batch that only led to a Vulcanian eruption (Fig 7D). If the ascent rate had been faster, as with the 1010 Cal. CE eruption, this may have resulted in a more explosive eruption. The absence of dome collapse during this small eruption suggests that pressure in the magma column overcome the load of the dome to produce a small explosive eruption (Fig 7D).

5.3.5 Implications for future eruptions and monitoring

This data suggests shows that explosive eruption style at La Soufrière is controlled by a combination of ascent rate and top-down controls and not necessarily linked exclusively to bottom-up processes, as highlighted by the Plinian eruptions studied here. Looking towards a future eruption, the various scenarios leading to explosive magmatic eruptions, and particularly the multiple controls on Plinian eruptions, make the La Soufrière volcanic system more hazardous and complex to forecast.

The results of this study have wider implications, not just for La Soufrière but for other systems with a developed hydrothermal system that tends to promote sealing of the host-rock, which influences the dynamics of magma ascent and degassing at shallow depth (e.g., Komorowski et al., 1997; 2010; in prep). To improve forecasting of potential future magmatic eruptions, continued development of volcano monitoring techniques must focus on developing the ability to: 1) reconstruct, via real-time geodesy, the deep stress field changes behind the upward movement of magma; 2) track the modifications of the physical properties of the host-rock; and 3) the development and evolution of sealing in the hydrothermal system. To understand the evolution of the magmatic system and how a potential eruption could evolve, monitoring should also keep tracking the petrology and rock properties of early erupted products, imaging the physio-chemical properties of the host-rock and its structures in time and space, and quantifying external forcing processes of the hydrothermal system that can modulate magma ascent dynamics. Particularly for volcanic systems with a wide range of eruptive behaviour, such as La Soufrière, this could provide a more complete understanding of how an eruption could develop and what its credible expected intensity might be.

6 Conclusions

The variation in eruption style at La Soufrière gives us opportunity to understand the controls on eruption explosivity at this volcano. The four eruptions discussed here are a Vulcanian (VEI 2), sub-Plinian (VEI 3) and two Plinian eruptions (VEI 4), covering a range of dominantly explosive magmatic activity produced by La Soufrière. Major and volatile elements of melt inclusions across the eruption series show the composition of the mush storage zone has remained stable. Melt inclusions also allow us to constrain the mush storage zone to 7 – 9 Km depth with an average temperature of 1000^{o}C. The constant composition and physical properties of the storage zone feeding the eruptions indicate that for some eruptions processes occurring from the top-down and external forces have also determined the magma ascent rate and controlled eruption style, particularly the intensity of the explosive activity.

Magma feeding the 1010 Cal. CE eruption ascended relatively rapidly (0.6 – 12 m/s) preventing the growth of microlites. The magma and exsolved gas remain coupled and ascended rapidly to trigger an explosive eruption style that was primarily driven by bottom-up processes. In contrast to the 1010 Cal. CE eruption, the 1657 Cal. CE eruption, where the magma ascended at a slower ascent rate (0.7 – 3 m/s), we find little geochemical and petrological evidence for any major top-down controls. This suggests the differences in ascent rate may have resulted in contrasting explosive eruption styles.

The magma feeding the 5680 Cal. BCE ascended comparatively slowly (0.04 -1 m/s) due to feedbacks between degassing and crystallization. These processes lead to an increase viscosity, further slowing magma ascent and promoting magma degassing. In the absence of any top-down controls this magma could have been expected to erupt with a low explosivity or effusively. However, sealing resulting from the capping dome and a reduction in permeability in the conduit favoured the accumulation of gas, leading to over pressurisation and an explosive Plinian eruption. External forces also played a role in the 1530 Cal. CE eruption where a flank collapse has resulted in rapid decompression of a gas-rich magma at shallow depth that rapidly led to a phase of sub-Plinian explosive activity at the onset of the multiphase eruption.

The multiple controls on explosive eruption style, and particularly on the most intense eruptions observed at La Soufrière, Plinian (VEI 4) eruptions, render this volcanic system particularly hazardous. Hence, the forecasting of the most credible eruption scenario is particularly challenging. Given that several eruption styles are possible and that eruption style can evolve within an eruption, we stress that monitoring efforts must also address the issue of tracking ascent and shallow-depth conduit processes which can influence eruption style, and particularly the intensity of explosivity. Given these uncertainties, we recommend that an integrated risk-reduction approach consider the capacity to detect rapid changes in unrest dynamics and associated eruption-driving processes, both at depth but also near the surface, and to develop associated preventive crisis response strategies on a short time frame.

7 Acknowledgements

The PhD scholarship of AM was co-funded by the “Make our Planet Great Again” initiative of the French Government (Campus France) and the IPGP Ecole Doctorale. We thank IPGP for general funding to the Observatoires Volcanologiques et Sismologiques (OVS), the INSU-CNRS for funding provided by Service National d'Observation en Volcanologie (SNOV), a Tellus-Aleas project to SM (2020, Insights into the dynamics of the active hydrothermal system of La Soufrière de Guadeloupe from past eruptions), and the Ministère pour la Transition Ecologique et Solidaire (MTES) for financial support. This work has been supported by the Clervolc (UCA-LMV), the AO-IPGP 2018 project “Depth to surface propagation of fluid-related anomalies at La Soufrière de Guadeloupe volcano (FWI): timing and implications for volcanic unrest” (coord.: R. Moretti), the project “Vers la Plateforme Régionale de Surveillance Tellurique du futur” (PREST) co-funded by INTERREG Caraïbes V for the European Regional Development Fund, and the European Union’s Horizon 2020 research and innovation programme, under grant agreement No 731070 (EUROVOLC project). This work was supported by the Institut National des Sciences de l’Univers (INSU-CNRS) for radiocarbon dating (AO Artemis, LMC14– CEA Saclay), and the CASAVA Project funded by Agence Nationale de la Recherche, 2009-2015 (ANR-09-RISK-02). The authors thank the OVSG-IPGP team for logistical support and help with data collection. We are grateful for help and information from Laurence and Eric Barret (Vert Intense). We thank Y. Legendre for assistance in the field and discussions over the geology of La Soufrière de Guadeloupe and the reconstruction of its eruptive past. We are grateful to the Parc National de Guadeloupe for allowing us to undertake research and obtain geological samples. We thank C. Martel for providing groundmass glass SEM images for the 1530 CE eruption. We are grateful for assistance in preparing samples and for analysis from Samia Hidalgo, Pierre Burckel, Stephan Borensztajn, Nicolas Rividi and Nicole Metrich. Radiocarbon dates were obtained from Beta Analytical. Finally, we would like to thank the two anonymous reviewers. This study contributes to the IdEx Université de Paris ANR-18-IDEX-0001 and is Laboratory of excellence ClerVolc contribution number 521 and IPGP contribution number **XXX**.

8 Author Contributions

AM prepared the samples, acquired the geochemical and petrological data, processed and analyzed all the data, wrote the draft of the manuscript and drafted the figures. J-CK, SM, and AM undertook fieldwork, and sampling. All authors discussed the data, wrote and revised the manuscript and the figures.

9 Figure Captions

Figure 1: Map of southern Basse-Terre showing the location of La Soufrière and volcanic complexes which make up the island. Also shown are sampling locations for each eruption.

Inset Left: Map showing the position of Guadeloupe in the Lesser Antilles Island arc chain. Inset Right: Image of La Soufrière (2020, Metcalfe).

Figure 2: Example images of glass from La Soufrière. **(A)** Plagioclase and **(B)** pyroxene hosted melt inclusions. Only inclusions with no daughter crystals analysed, inclusions can be round and uniform or more irregular. Plagioclase often shows primary and secondary inclusions, only inclusions from the core of the crystal which are primary inclusions were analysed. **(C-E)** Pyroxene hosted inclusions (C – 5680 Cal. BCE, D – 1010 Cal CE, E – 1657 Cal CE) (**F-H)** Plagioclase hosted inclusions (F – 5680 Cal. BCE, G – 1010 Cal CE, H – 1657 Cal CE). **(I-N)** Groundmass glass (I – 5680 Cal. BCE, J – 1010 Cal CE (Legendre, 2012), K – 1657 Cal CE (Legendre, 2012), L – 1530 Cal CE (light glass) (Martel et al., 2021), M – 1530 Cal CE (dark glass) (Martel et al., 2021), N - 1530 Cal CE (homogenous glass) (Martel et al., 2021).

Figure 3: Total Alkali-Silica whole rock dataset for the La Soufrière eruptions and parental Monts Caraïbes magma. The groundmass glass show some Na_2O loss during analysis. Generally, the data falls on the same liquid-line of descent.

Figure 4: Complete major element data set: (A) FeO, (B) CaO, (C) K_2O, (D) MnO, (E) MgO, (F) Al_2O_3, (G) Na_2O, (H) TiO_2 vs SiO_2.

Figure 5: Volatile contents for melt inclusion and: (A) H_2O, (B) CO_2, (C) S, (D) Cl, (E) F vs K_2O and (F) Total Volatile Content vs VEI. Data is clustered with no significant difference in the volatile contents for each eruption.

Figure 6: Eruption year vs (A) Temperature (Putirka, 2008), (B) Pressure (Papale et al., 2006, errors calculated based on model error and volatile analysis error), (C) Viscosity (groundmass (GM) and groundmass with microlites (GM+X), Mastin, 2002), (D) Ascent Rate (Mastin, 2002).

Figure 7: Schematic diagram of the La Soufrière reservoir for each eruption discussed, with calculated parameters annotated. **(A)** 5680 Cal. BCE (VEI 4): eruptible melt from 9 km depth begins ascending in the conduit at max. 1 m/s. The slow ascent results in feedbacks between degassing and crystallization increasing viscosity and slowing ascent further. Sealing of the conduit from the top-down due to the presence of a dome results in exsolved volatile accumulation and pressure increases, until the overpressure exceeds the strength of the confining rock and the seal fails resulting in a Plinian eruption. **(B)** 1010 Cal. CE (VEI 4): eruptible melt from 6 Km depth begins ascending in the conduit at max. 12 m/s. Volatile exsolution has prevented a large viscosity change but increased buoyancy allowing the magma to rise. Disequilibrium closed system degassing has driven magma still coupled to the melt from the bottom up allowing fast ascent resulting in a Plinian eruption. **(C)** 1530 Cal. CE (VEI 3): magma from the supply system moves up into the storage zone resulting in

magma mixing. Eruptible melt from 7 Km depth begins ascending in the conduit at 2-4 m/s, with microlite textures reveal a complex ascent history. A flank collapse has rapidly released the edifice load resulting in a downward propagating pressure change which affects the decompression rate of the magma resulting in fragmentation a sub-Plinian explosion. **(D)** 1657 Cal. CE (VEI 2): eruptible melt from 8 Km depth begins ascending in the conduit at max 3 m/s, the slower ascent compared to the 1010 CE eruption and without influence from top down processes, has resulted in a Vulcanian explosion. The dome did not collapse during this small eruption.

10 References

Alidibirov, M. and Dingwell, D.B., 1996. Magma fragmentation by rapid decompression. *Nature*, *380*(6570), pp.146-148.

Allard, P. (2010). A CO2-rich gas trigger of explosive paroxysms at Stromboli basaltic volcano, Italy. Journal of Volcanology and Geothermal Research, 189(3-4), 363-374.

Allard P, Aiuppa A, Beauducel F, Gaudin D, Di Napoli R, Calabrese S, Parello F, Crispi O, Hammouya and Tamburello G (2014). Steam and gas emission rate from La Soufrière volcano, Guadeloupe (Lesser Antilles): Implications for the magmatic supply during degassing unrest. *Chemical Geology*, 384, pp.76-93.

Allison, C. M., Roggensack, K., & Clarke, A. B. (2021). Highly explosive basaltic eruptions driven by CO 2 exsolution. Nature communications, 12(1), 1-10.

Anderson, A.T. and Brown, G.G., 1993. CO2 contents and formation pressures of some Kilauean melt inclusions. *American Mineralogist*, *78*(7-8), pp.794-803.

Anderson JR, A.T., 1974. Evidence for a picritic, volatile-rich magma beneath Mt. Shasta, California. *Journal of Petrology*, *15*(2), pp.243-267.

Anderson, S.W., Fink, J.H. and Rose, W.I., 1995. Mount St. Helens and Santiaguito lava domes: the effect of short-term eruption rate on surface texture and degassing processes. *Journal of Volcanology and Geothermal Research*, *69*(1-2), pp.105-116.

Annen, C., Blundy, J.D., Leuthold, J. and Sparks, R.S.J., 2015. Construction and evolution of igneous bodies: Towards an integrated perspective of crustal magmatism. *Lithos*, *230*, pp.206-221.

Atlas, Z.D., Dixon, J.E., Sen, G., Finny, M. and Martin-Del Pozzo, A.L., 2006. Melt inclusions from Volcán Popocatépetl and Volcán de Colima, Mexico: melt evolution due to vapor-saturated crystallization during ascent. *Journal of Volcanology and Geothermal Research*, *153*(3-4), pp.221-240.

Arzilli, F., La Spina, G., Burton, M.R., Polacci, M., Le Gall, N., Hartley, M.E., Di Genova, D., Cai, B., Vo, N.T., Bamber, E.C. and Nonni, S., 2019. Magma fragmentation in highly explosive basaltic eruptions induced by rapid crystallization. *Nature Geoscience*, *12*(12), pp.1023-1028.

Assbichler, D. (2020). Impact of CO_2 on alkali-rich explosive volcanism. Doctoral dissertation, Ludwig Maximilien University (D), 183 pp.

Bachmann, O., Dungan, M. A., Lipman, P. W. (2002). The Fish Canyon magma body, San Juan volcanic field, Colorado: rejuvenation and eruption of an upper-crustal batholith. *Journal of Petrology*, 43, pp. 1469-15

Barberi, F., Bertagnini, A., Landi, P. and Principe, C., 1992. A review on phreatic eruptions and their precursors. *Journal of volcanology and geothermal research*, *52*(4), pp.231-246.

Barmin, A., Melnik, O. and Sparks, R.S.J., 2002. Periodic behavior in lava dome eruptions. *Earth and Planetary Science Letters*, *199*(1-2), pp.173-184.

Barsanti, M., Papale, P., Barbato, D., Moretti, R., Boschi, E., Hauri, E., & Longo, A. (2009). Heterogeneous large total CO_2 abundance in the shallow magmatic system of Kilauea volcano, Hawaii. Journal of Geophysical Research: Solid Earth, 114(B12).

Barth, A., Newcombe, M., Plank, T., Gonnermann, H., Hajimirza, S., Soto, G.J., Saballos, A. and Hauri, E., 2019. Magma decompression rate correlates with explosivity at basaltic volcanoes—Constraints from water diffusion in olivine. *Journal of Volcanology and Geothermal Research*, *387*, p.106664.

Bergantz, G.W., Schleicher, J.M. and Burgisser, A., 2015. Open-system dynamics and mixing in magma mushes. *Nature Geoscience*, *8*(10), pp.793-796.

Bergantz, G.W., Schleicher, J.M. and Burgisser, A., 2017. On the kinematics and dynamics of crystal-rich systems. *Journal of Geophysical Research: Solid Earth*, *122*(8), pp.6131-6159.

Bernard, O. and de Maisonneuve, C.B., 2020. Controls on eruption style at Rabaul, Papua New Guinea–Insights from microlites, porosity and permeability measurements. *Journal of Volcanology and Geothermal Research*, *406*, p.107068.

Bissainte M (1995). Le complexe des Monts Caraïbes de Guadeloupe (Arc des Petites Antilles) Etude pétrographique, minéralogique et géochimique. Ph.D. thesis, Paris.

Blundy, J. and Cashman, K., 2005. Rapid decompression-driven crystallization recorded by melt inclusions from Mount St. Helens volcano. *Geology*, *33*(10), pp.793-796.

Blundy, J., Cashman, K.V., Rust, A. and Witham, F., 2010. A case for CO2-rich arc magmas. *Earth and Planetary Science Letters*, *290*(3-4), pp.289-301.

Bodnar, R.J., Binns, P.R. and Hall, D.L., 1989. Synthetic fluid inclusions-VI. Quantitative evaluation of the decrepitation behaviour of fluid inclusions in quartz at one atmosphere confining pressure. *Journal of Metamorphic Geology*, *7*(2), pp.229-242.

Borgia, A., Tizzani, P., Solaro, G., Manzo, M., Casu, F., Luongo, G., Pepe, A., Berardino, P., Fornaro, G., Sansosti, E. and Ricciardi, G.P., 2005. Volcanic spreading of Vesuvius, a new paradigm for interpreting its volcanic activity. *Geophysical Research Letters*, *32*(3).

Boudon, G., Balcone-Boissard, H., Villemant, B. and Morgan, D.J., 2015. What factors control superficial lava dome explosivity?. *Scientific reports*, *5*(1), pp.1-14.

Boudon G, Komorowski JC, Villemant B and Semet M (2008). A new scenario for the last magmatic eruption of La Soufrière de Guadeloupe (Lesser Antilles) in 1530 A.D. Evidence from stratigraphy radiocarbon dating and magmatic evolution of erupted products. *Journal of Volcanology and Geothermal Research*, 178(3), pp.474-490.

1167 Boudon, G., Le Friant, A., Komorowski, J.C., Deplus, C. and Semet, M.P., 2007. Volcano flank
1168 instability in the Lesser Antilles Arc: Diversity of scale, processes, and temporal recurrence. *Journal*
1169 *of Geophysical Research: Solid Earth*, *112*(B8).

1170 Boudon, G., Semet, M.P., Komorowski, J.C., Villemant, B. and Michel, A., 2003, April. Was the last
1171 magmatic eruption of la Soufrière, Guadeloupe, in 1440 AD, triggered by partial collapse of the
1172 volcano?. In *EGS-AGU-EUG Joint Assembly*(p. 10398).

1173 Boudon, G., Le Friant, A., Komorowski, J.C., Deplus, C. and Semet, M.P., 2007. Volcano flank
1174 instability in the Lesser Antilles Arc: Diversity of scale, processes, and temporal recurrence. *Journal*
1175 *of Geophysical Research: Solid Earth*, *112*(B8).

1176 Bourgeoisat C (2018). Spatio-temporal dynamics of the magmatic reservoir at the origin of the 1530
1177 AD eruption of La Soufrière of Guadeloupe. Master's thesis, Paris.

1178 Bouvet De Maisonneuve, C., Dungan, M.A., Bachmann, O. and Burgisser, A., 2013. Petrological
1179 insights into shifts in eruptive styles at Volcán Llaima (Chile). *Journal of Petrology*, *54*(2), pp.393-420.

1180 Bower, S.M. and Woods, A.W., 1996. On the dispersal of clasts from volcanic craters during small
1181 explosive eruptions. *Journal of Volcanology and Geothermal Research*, *73*(1-2), pp.19-32.

1182 Brown, R. J., Civetta, L., Arienzo, I., D'Antonio, M., Moretti, R., Orsi, G., G. and Tomlinson, E.L., Albert,
1183 P.G., Menzies, M. A. (2014). Geochemical and isotopic insights into the assembly, evolution and
1184 disruption of a magmatic plumbing system before and after a cataclysmic caldera-collapse eruption
1185 at Ischia volcano (Italy). *Contributions to Mineralogy and Petrology*, 168, 1035.

1186 Burgisser A and Bergantz G (2011). A rapid mechanism to remobilize and homogenize highly
1187 crystalline magma bodies. *Nature*, 471(7337), pp.212-215.

1188 Burgisser, A., Arbaret, L., Druitt, T.H. and Giachetti, T., 2011. Pre-explosive conduit conditions of the
1189 1997 Vulcanian explosions at Soufrière Hills Volcano, Montserrat: II. Overpressure and depth
1190 distributions. *Journal of Volcanology and Geothermal Research*, *199*(3-4), pp.193-205.

1191 Campbell, A.J., Danielson, L., Righter, K., Seagle, C.T., Wang, Y. and Prakapenka, V.B., 2009. High
1192 pressure effects on the iron–iron oxide and nickel–nickel oxide oxygen fugacity buffers. *Earth and*
1193 *Planetary Science Letters*, *286*(3-4), pp.556-564.

1194 Cappello, A., Ganci, G., Bilotta, G., Corradino, C., Hérault, A. and Del Negro, C., 2019. Changing
1195 eruptive styles at the south-east crater of Mount Etna: Implications for assessing lava flow
1196 hazards. *Frontiers in Earth Science*, *7*, p.213.

1197 Carrara A, Burgisser A and Bergantz G (2019). Lubrication effects on magmatic mush
1198 dynamics. *Journal of Volcanology and Geothermal Research*, 380, pp.19-30.

1199 Cashman, K. and Blundy, J., 2000. Degassing and crystallization of ascending andesite and
1200 dacite. *Philosophical Transactions of the Royal Society of London. Series A: Mathematical, Physical*
1201 *and Engineering Sciences*, *358*(1770), pp.1487-1513.

1202 Cashman K, Sparks R and Blundy J (2017). Vertically extensive and unstable magmatic systems: A
1203 unified view of igneous processes. *Science*, 355(6331) pp 3055

1204 Cashman, K.V., 2004. Volatile controls on magma ascent and eruption. *The State of the Planet:*
1205 *Frontiers and Challenges in Geophysics*, *150*, pp.109-124.

Cassidy, M., Castro, J.M., Helo, C., Troll, V.R., Deegan, F.M., Muir, D., Neave, D.A. and Mueller, S.P., 2016. Volatile dilution during magma injections and implications for volcano explosivity. *Geology*, *44*(12), pp.1027-1030.

Cassidy, M., Manga, M., Cashman, K. and Bachmann, O., 2018. Controls on explosive-effusive volcanic eruption styles. *Nature communications*, *9*(1), pp.1-16.

Castro, J.M. and Gardner, J.E., 2008. Did magma ascent rate control the explosive-effusive transition at the Inyo volcanic chain, California?. *Geology*, *36*(4), pp.279-282.

Cheng L, Costa F and Bergantz G (2020). Linking fluid dynamics and olivine crystal scale zoning during simulated magma intrusion. *Contributions to Mineralogy and Petrology*, 175(6).

Cioni, R., Bertagnini, A., Santacroce, R. and Andronico, D., 2008. Explosive activity and eruption scenarios at Somma-Vesuvius (Italy): towards a new classification scheme. *Journal of Volcanology and Geothermal Research*, *178*(3), pp.331-346.

Clarke, A.B., Neri, A., Voight, B., Macedonio, G. and Druitt, T.H., 2002. Computational modelling of the transient dynamics of the August 1997 Vulcanian explosions at Soufriere Hills Volcano, Montserrat: influence of initial conduit conditions on near-vent pyroclastic dispersal. *MEMOIRS-GEOLOGICAL SOCIETY OF LONDON*, *21*, pp.319-348.

Coltelli, M., Del Carlo, P., Pompilio, M. and Vezzoli, L., 2005. Explosive eruption of a picrite: The 3930 BP subplinian eruption of Etna volcano (Italy). *Geophysical Research Letters*, *32*(23).

Colucci, S., Vitturi, M.D.M., Neri, A. and Palladino, D.M., 2014. An integrated model of magma chamber, conduit and column for the analysis of sustained explosive eruptions. *Earth and Planetary Science Letters*, *404*, pp.98-110.

Cooper K (2019). Time scales and temperatures of crystal storage in magma reservoirs: implications for magma reservoir dynamics. *Philosophical Transactions of the Royal Society A: Mathematical, Physical and Engineering Sciences*, 377(2139), p.20180009.

Cooper, K.M. and Kent, A.J., 2014. Rapid remobilization of magmatic crystals kept in cold storage. *Nature*, *506*(7489), pp.480-483.

Costa, F., Lara, L., Kyriazis, S.F., Vazquez, J. and Cembrano, J., 2009, April. Time scales and petrogenesis of silicic magmas. In *EGU General Assembly Conference Abstracts* (p. 4124).

Costa F, Andreastuti S, Bouvet de Maisonneuve C and Pallister J (2013). Petrological insights into the storage conditions, and magmatic processes that yielded the centennial 2010 Merapi explosive eruption. *Journal of Volcanology and Geothermal Research*, 261, pp.209-235.

Danyushevsky, L.V., McNeill, A.W. and Sobolev, A.V., 2002. Experimental and petrological studies of melt inclusions in phenocrysts from mantle-derived magmas: an overview of techniques, advantages and complications. *Chemical Geology*, *183*(1-4), pp.5-24.

Degruyter, W., Huber, C., Bachmann, O., Cooper, K.M. and Kent, A.J., 2016. Magma reservoir response to transient recharge events: The case of Santorini volcano (Greece). *Geology*, *44*(1), pp.23-26.

De Natale, G., Troise, C., Trigila, R., Dolfi, D., & Chiarabba, C. (2004). Seismicity and 3-D substructure at Somma–Vesuvius volcano: evidence for magma quenching. Earth and Planetary Science Letters, 221(1-4), 181-196.

Devine, J.D., Rutherford, M.J. and Gardner, J.E., 1998. Petrologic determination of ascent rates for the 1995–1997 Soufriere Hills Volcano andesitic magma. *Geophysical Research Letters*, *25*(19), pp.3673-3676.

Dingwell, D.B., 1996. Volcanic Dilemma--Flow or Blow?. *Science*, *273*(5278), pp.1054-1055.

Edmonds, M., Aiuppa, A., Humphreys, M., Moretti, R., Giudice, G., Martin, R.S., Herd, R.A. and Christopher, T., 2010. Excess volatiles supplied by mingling of mafic magma at an andesite arc volcano. *Geochemistry, Geophysics, Geosystems*, *11*(4).

Edmonds M, Kohn S, Hauri E, Humphreys M and Cassidy M (2016). Extensive, water-rich magma reservoir beneath southern Montserrat. *Lithos*, 252-253, pp.216-233.

Edmonds, M. and Wallace, P.J., 2017. Volatiles and exsolved vapor in volcanic systems. *Elements*, *13*(1), pp.29-34.

Endo, E., Malone, S., Noson, L. & Weaver, C. (1981) The 1980 Eruptions of Mount St. Helens, Washington 93–108, professional paper 1250 (U.S. G.P.O., Washington, DC, 1981).

Esposti Ongaro, T., Komorowski, J-C., Legendre, Y., Neri, A. (2020) Modelling pyroclastic density currents from a subplinian eruption at La Soufrière de Guadeloupe (West Indies), Bulletin of Volcanology, 82:76, https://doi.org/10.1007/s00445-020-01411-6

Fedotov, S.A., 1981. Magma rates in feeding conduits of different volcanic centres. *Journal of Volcanology and Geothermal Research*, *9*(4), pp.379-394.

Feuillard M, Allegre C, Brandeis G, Gaulon R, Le Mouel J, Mercier J, Pozzi J and Semet M (1983). The 1975–1977 crisis of La Soufrière de Guadeloupe (F.W.I): A still-born magmatic eruption. *Journal of Volcanology and Geothermal Research*, 16(3-4), pp.317-334.

Gaetani, G.A. and Watson, E.B., 2000. Open system behavior of olivine-hosted melt inclusions. *Earth and Planetary Science Letters*, *183*(1-2), pp.27-41.

Ghiorso, M.S. and Sack, R.O., 1995. Chemical mass transfer in magmatic processes IV. A revised and internally consistent thermodynamic model for the interpolation and extrapolation of liquid-solid equilibria in magmatic systems at elevated temperatures and pressures. *Contributions to Mineralogy and Petrology*, *119*(2), pp.197-212.

Ghiorso, M.S. and Gualda, G.A., 2015. An H 2 O–CO 2 mixed fluid saturation model compatible with rhyolite-MELTS. *Contributions to Mineralogy and Petrology*, *169*(6), pp.1-30.

Goepfert, K. and Gardner, J.E., 2010. Influence of pre-eruptive storage conditions and volatile contents on explosive Plinian style eruptions of basic magma. *Bulletin of Volcanology*, *72*(5), pp.511-521.

Gonnermann, H. M. (2015). Magma fragmentation. Annual Review of Earth and Planetary Sciences, 43, 431-458.

Gonnermann, H.M. and Manga, M., 2007. The fluid mechanics inside a volcano. *Annu. Rev. Fluid Mech.*, *39*, pp.321-356.

Gonnermann, H.M. and Manga, M., 2013. Dynamics of magma ascent. *Modeling volcanic processes: The physics and mathematics of volcanism*, pp.55-84.

Gualda, G.A., Ghiorso, M.S., Lemons, R.V. and Carley, T.L., 2012. Rhyolite-MELTS: a modified calibration of MELTS optimized for silica-rich, fluid-bearing magmatic systems. *Journal of Petrology*, *53*(5), pp.875-890.

Gottsmann, J., Komorowski, J-C., Barclay, J. (2019) Chapter 1 : Volcanic unrest and pre-eruptive processes : A hazard and risk perspective. In : J. Gottsmann, J. Neuberg, B. Scheu (Eds), Volcanic Unrest - From Science to Society, Advances in Volcanology, p.1–21, Springer-Verlag Berlin Heidelberg, eBoob ISBN : 978-3-319-58412-6 ; Hardcover ISBN : 978-3-319-58411-9, DOI 10.1007/11157_2017_19

Heap, M.J., Bauman, T.S., Rosas-Carbajal, M., Komorowski, J-C., Gilg, A.H., Villeneuve, M., Moretti, R., Baud, P., Carbillet, L., Harnett, C., Reuschlé, T. (2021) Alteration-induced volcano instability at La Soufrière de Guadeloupe (Eastern Caribbean), Journal of Geophysical Research, in press

Hincks, T., Komorowski J-C, R.S.J. Sparks, W.P. Aspinall. (2014) Retrospective analysis of uncertain eruption precursors at La Soufrière volcano, Guadeloupe, 1975-77 : volcanic hazard assessment using a Bayesian Belief Network approach. Journal of Applied Volcanology, 3 :3 ; 10.1186/2191-5040-3-3 ; http://www.appliedvolc.com/content/3/1/3

Hlinka, L "Top–Down Control on Eruptive Style at Masaya Volcano Inferred from Melt Composition" (2020). *CUNY Academic Works.* Ph.D. thesis, Queens College.

Hlinka, L., Longpré, M.A., Pérez, W., Kutterolf, S. and Monteleone, B., 2021. Top–down control on eruptive style at Masaya volcano inferred from melt composition. *Earth and Planetary Science Letters*, *572*, p.117138.

Hauri, E., 2002. SIMS analysis of volatiles in silicate glasses, 2: isotopes and abundances in Hawaiian melt inclusions. *Chemical Geology*, *183*(1-4), pp.115-141.

Heap, M.J., Troll, V.R., Kushnir, A.R., Gilg, H.A., Collinson, A.S., Deegan, F.M., Darmawan, H., Seraphine, N., Neuberg, J. and Walter, T.R., 2019. Hydrothermal alteration of andesitic lava domes can lead to explosive volcanic behaviour. *Nature communications*, *10*(1), pp.1-10.

Heap, M., Baumann, T., Rosas-Carbajal, M., Komorowski, J.C., Gilg, H.A., Villeneuve, M., Moretti, R., Baud, P., Carbillet, L., Harnett, C. and Reuschlé, T., 2021, April. The influence of hydrothermal alteration on volcano stability: a case study of La Soufrière de Guadeloupe (France). In *EGU General Assembly Conference Abstracts* (pp. EGU21-151).

Helo, C., Longpré, M.A., Shimizu, N., Clague, D.A. and Stix, J., 2011. Explosive eruptions at mid-ocean ridges driven by CO 2-rich magmas. *Nature Geoscience*, *4*(4), pp.260-263.

Houghton, B.F. and Gonnermann, H.M., 2008. Basaltic explosive volcanism: constraints from deposits and models. *Geochemistry*, *68*(2), pp.117-140.

Huppert, H.E. and Woods, A.W., 2002. The role of volatiles in magma chamber dynamics. *Nature*, *420*(6915), pp.493-495.

Jackson, M., Blundy, J. and Sparks, R., (2018). Chemical differentiation, cold storage and remobilization of magma in the Earth's crust. *Nature*, 564(7736), pp.405-409.

1321 Johnson, E.R., Wallace, P.J., Cashman, K.V. and Granados, H.D., 2010. Degassing of volatiles (H2O,
1322 CO2, S, Cl) during ascent, crystallization, and eruption at mafic monogenetic volcanoes in central
1323 Mexico. *Journal of Volcanology and Geothermal Research*, *197*(1-4), pp.225-238.

1324 Kilgour, G., Blundy, J., Cashman, K. and Mader, H.M., 2013. Small volume andesite magmas and
1325 melt–mush interactions at Ruapehu, New Zealand: evidence from melt inclusions. *Contributions to*
1326 *Mineralogy and Petrology*, *166*(2), pp.371-392.

1327 Komorowski, J-C., Hoblitt, R.P., Sheridan, M.F., 1997. Silicification and brecciation microtextures of
1328 the Mt. St. Helens'1980 cryptodome-country rock interface: implications for hydrothermal fluid
1329 processes, precursory seismicity, and eruptive style. International Association of Volcanology and
1330 Chemistry of the Earth's Interior, General Assembly, Puerto Vallarta, Mexico, Jan. 19-25 1997,
1331 Abstract, p. 76.

1332 Komorowski J-C, G. Boudon, M. Semet, F. Beauducel, C. Anténor-Habazac, S. Bazin, G. Hammouya.
1333 Guadeloupe. (2005) In: J.M. Lindsay, R.E.A. Robertson, J.B. Shepherd & S. Ali (Eds), Volcanic Hazard
1334 Atlas of the Lesser Antilles, Seismic Research Uni, The University of the West Indies, Trinidad and
1335 Tobago, WI, 65-102.

1336 Komorowski J-C, Legendre Y., Caron B., Boudon G. (2008). Reconstruction and analysis of sub-Plinian
1337 tephra dispersal during the 1530 A.D. Soufrière (Guadeloupe) eruption: implications for scenario
1338 definition and hazards assessment J. Volcanol. Geotherm. Res. 178: 491-515

1339 Komorowski J-C., Legendre, Y., Christopher, T., Bernstein, L., R. Stewart, Joseph, E., Fournier, N.,
1340 Chardot, L., Finizola, A., Wadge, G., Syers, R., Williams, C, Bass, V. (2010), Insights into processes and
1341 deposits of hazardous vulcanian explosions at Soufrière Hills Volcano during 2008 and 2009
1342 (Montserrat, West Indies), Geophys. Res. Lett., 37, L00E19, doi :10.1029/2010GL042558

1343 Komorowski J-C, Legendre Y, Boudon G et al (2012) A new Holocene eruptive chronology for La
1344 Soufrière of Guadeloupe volcano: implications for credible scenario definition as well as hazard and
1345 impact modelling. Cities on Volcanoes 7, 18-23 November 2012, IAVCEI, Colima, Mexico

1346 Komorowski, J-C, Legendre Y, Barsotti S (2013) Assessing long term hazards for La Soufrière of
1347 Guadeloupe volcano: insights from a new eruptive chronology, credible scenario definition, and
1348 integrated impact modelling. International Association of Volcanology and Chemistry of the Earth's
1349 Interior (IAVCEI), Scientific Assembly, Kagoshima, Japan, 19-24 July 2013, abstract, 4W_4D-P1

1350 Komorowski J-C, Jenkins, S., Baxter, P., Picquout, A., Lavigne, F., Charbonnier, S.J., Gertisser, R., K.
1351 Preece, Cholik, N., Budi-Santoso, A., Surono. (2013) Paroxysmal dome explosion during the Merapi
1352 2010 eruption : Processes and facies relationships of associated high-energy pyroclastic density
1353 currents. Jour. Volcanol. Geotherm. Res., 261, 260–294,
1354 http://dx.doi.org/10.1016/j.jvolgeores.2013.01.007

1355 Komorowski, J-C., Hoblitt, R.P., Sheridan, M.F., Heap, M.J., Wadsworth, F.B. (In prep). Tuffisites at
1356 the Mt St Helens 1980 cryptodome-host rock interface: implications for fluid circulation, volcano
1357 stability, and pre-eruptive seismicity. Journal of Volcanology and Geothermal Research (in prep).

1358 Kress, V.C. and Carmichael, I.S., 1991. The compressibility of silicate liquids containing Fe 2 O 3 and
1359 the effect of composition, temperature, oxygen fugacity and pressure on their redox
1360 states. *Contributions to Mineralogy and Petrology*, *108*(1), pp.82-92.

1361 Kyser, T.K. and O'Neil, J.R., 1984. Hydrogen isotope systematics of submarine basalts. *Geochimica et*
1362 *Cosmochimica Acta*, *48*(10), pp.2123-2133.

1363 Lautze, N.C. and Houghton, B.F., 2007. Linking variable explosion style and magma textures during
1364 2002 at Stromboli volcano, Italy. *Bulletin of Volcanology*, *69*(4), pp.445-460.

1365 Lavallée, Yan, P. M. Benson, M. J. Heap, Asher Flaws, K-U. Hess, and Donald B. Dingwell. "Volcanic
1366 conduit failure as a trigger to magma fragmentation." *Bulletin of volcanology* 74, no. 1 (2012): 11-13.

1367 Le Guern, F., Bernard, A. and Chevrier, R.M., 1980. Soufriere of Guadeloupe 1976–1977 eruption—
1368 Mass and energy transfer and volcanic health hazards. *Bulletin volcanologique*, *43*(3), pp.577-593.

1369 Legendre Y (2012). Reconstruction de l'histoire éruptive et scenarii éruptifs à La Soufrière de
1370 Guadeloupe: vers un modèle intégral de fonctionnement du volcan. (French) [A high resolution
1371 reconstruction of the eruptive past and definition of eruptive scenario at La Soufrière of
1372 Guadeloupe]. Ph.D. thesis, Paris.

1373 Leone, F., Komorowski, J-C, Gherardi-Leone, M., Lalubie, G. (2019). Integrating spatial accessibility in
1374 the design of "volcano" evacuation plans: application in the French West Indies (Guadeloupe and
1375 Martinique). Journal of Applied Volcanology, 8 :8, 1-22 pp, , https://doi.org/10.1186/s13617-019-
1376 0089-1

1377 Lloyd, A.S., Ruprecht, P., Hauri, E.H., Rose, W., Gonnermann, H.M. and Plank, T., 2014. NanoSIMS
1378 results from olivine-hosted melt embayments: Magma ascent rate during explosive basaltic
1379 eruptions. *Journal of Volcanology and Geothermal Research*, *283*, pp.1-18.

1380 Lowenstern, J.B., 1995. Applications of silicate-melt inclusions to the study of magmatic
1381 volatiles. *Magmas, fluids, and ore deposits*, *23*, pp.71-99.

1382 Mader, H.M., Llewellin, E.W. and Mueller, S.P., 2013. The rheology of two-phase magmas: A review
1383 and analysis. *Journal of Volcanology and Geothermal Research*, *257*, pp.135-158.

1384 Mahood, G.A., 1990. Evidence for long residence times of rhyolitic magma in the Long Valley
1385 magmatic system-The isotopic record in the precaldera lavas of Glass Mountain-Reply. *Earth and*
1386 *Planetary Science Letters*, *99*(4), pp.395-399.

1387 Mangan, M.T., Sisson, T.W. and Hankins, W.B., 2004. Decompression experiments identify kinetic
1388 controls on explosive silicic eruptions. *Geophysical Research Letters*, *31*(8).

1389 Martel, C., 2012. Eruption dynamics inferred from microlite crystallization experiments: application
1390 to Plinian and dome-forming eruptions of Mt. Pelée (Martinique, Lesser Antilles). *Journal of*
1391 *Petrology*, *53*(4), pp.699-725.

1392 Martel, C., Pichavant, M., Balcone-Boissard, H. and Boudon, G., Syn-eruptive conditions of the AD
1393 1530 sub-Plinian eruption of La Soufrière of Guadeloupe (Lesser Antilles). *Frontiers in Earth Science*,
1394 p.1082.

1395 Mastin, L.G. and Ghiorso, M.S., 2001. Adiabatic temperature changes of magma–gas mixtures during
1396 ascent and eruption. *Contributions to Mineralogy and Petrology*, *141*(3), pp.307-321.

1397 Mastin, L.G., 2002. Insights into volcanic conduit flow from an open-source numerical
1398 model. *Geochemistry, Geophysics, Geosystems*, *3*(7), pp.1-18.

Melnik, O. and Sparks, R.S.J., 1999. Nonlinear dynamics of lava dome extrusion. *Nature*, *402*(6757), pp.37-41.

Melnik, O. and Sparks, R.S.J., 2002. Dynamics of magma ascent and lava extrusion at Soufrière Hills Volcano, Montserrat. *Geological Society, London, Memoirs*, *21*(1), pp.153-171.

Metcalfe A, Moune S, Komorowski J-C, Kilgour G, Jessop DE, Moretti R and Legendre Y (2021) Magmatic Processes at La Soufrière de Guadeloupe: Insights From Crystal Studies and Diffusion Timescales for Eruption Onset. Front. Earth Sci. 9:617294. doi: 10.3389/feart.2021.617294

Moitra, P., Gonnermann, H.M., Houghton, B.F. and Tiwary, C.S., 2018. Fragmentation and Plinian eruption of crystallizing basaltic magma. *Earth and Planetary Science Letters*, *500*, pp.97-104.

Moretti, R., & Papale, P. (2004). On the oxidation state and volatile behavior in multicomponent gas–melt equilibria. Chemical Geology, 213(1-3), 265-280.

Moretti, R., Métrich, N., Arienzo, I., Di Renzo, V., Aiuppa, A., & Allard, P. (2018). Degassing vs. eruptive styles at Mt. Etna volcano (Sicily, Italy). Part I: Volatile stocking, gas fluxing, and the shift from low-energy to highly explosive basaltic eruptions. Chemical Geology, 482, 1-17.

Moretti R., Arienzo I., Civetta L., Orsi G, D'Antonio M. (2013) The deep plumbing system of the Ischia island: a physico-chemical window on the fluid-saturated and CO_2-sustained Neapolitan volcanism (Southern Italy). *Journal of Petrology*, 54, pp. 951-984

Moretti, R., Arienzo, I., Di Renzo, V., Orsi, G., Arzilli, F., Brun, F., D'Antonio, M., Mancini, L., Deloule, E. (2019). Volatile segregation and generation of highly vesiculated explosive magmas by volatile-melt fining processes: The case of the Campanian Ignimbrite eruption. Chemical Geology, 503, pp. 1-14.

Moretti R, Komorowski JC, Ucciani G, Moune S, Jessop DE, de Chabalier J, Beauducel F, Bonifacie M, Burtin A, Vallée M, Deroussi S, Robert V, Gibert D, Didier T, Kitou T, Feuillet N, Allard P, Tamburello G, Shreve T, Saurel J, Lemarchand A, Rosas-Carbajal M, Agrinier P, Le Friant A and Chaussidon M (2020). The 2018 unrest phase at La Soufrière de Guadeloupe (French West Indies) andesitic volcano: Scrutiny of a failed but prodromal phreatic eruption. *Journal of Volcanology and Geothermal Research*, 393, p.106769.

Moune S, Moretti R, Burtin A, Jessop. D.E, Didier T, Robert V, Bonifacie M, Tamburello G, Komorowski J-C, Allard P, Buscetti M (2022). Gas monitoring of volcanic-hydrothermal plumes in a tropical environment: the case of La Soufrière de Guadeloupe unrest volcano (FWI). *In press: Frontiers in Earth Science.*

Mujin, M. and Nakamura, M., 2020. Late-stage groundmass differentiation as a record of magma stagnation, fragmentation, and rewelding. *Bulletin of Volcanology*, *82*, pp.1-17.

Nakamura, M. (1995). Continuous mixing of crystal mush and replenished magma in the ongoing Unzen eruption. *Geology*, 23, pp. 807-810.

Navelot, V., Géraud, Y., Favier, A., Diraison, M., Corsini, M., Lardeaux, J.M., Verati, C., de Lepinay, J.M., Legendre, L. and Beauchamps, G., 2018. Petrophysical properties of volcanic rocks and impacts of hydrothermal alteration in the Guadeloupe Archipelago (West Indies). *Journal of Volcanology and Geothermal Research*, *360*, pp.1-21.

1438 Owen, J., Tuffen, H. and McGarvie, D.W., 2013. Explosive subglacial rhyolitic eruptions in Iceland are
1439 fuelled by high magmatic H2O and closed-system degassing. *Geology*, *41*(2), pp.251-254.

1440 Papale, P. and Dobran, F., 1994. Magma flow along the volcanic conduit during the Plinian and
1441 pyroclastic flow phases of the May 18, 1980, Mount St. Helens eruption. *Journal of Geophysical*
1442 *Research: Solid Earth*, *99*(B3), pp.4355-4373.

1443 Papale, P., Moretti, R. and Barbato, D., 2006. The compositional dependence of the saturation
1444 surface of H2O+ CO2 fluids in silicate melts. *Chemical Geology*, *229*(1-3), pp.78-95.

1445 Papale, P., 1999. Strain-induced magma fragmentation in explosive eruptions. *Nature*, *397*(6718),
1446 pp.425-428.

1447 Papale, P. and Polacci, M., 1999. Role of carbon dioxide in the dynamics of magma ascent in
1448 explosive eruptions. *Bulletin of volcanology*, *60*(8), pp.583-594.

1449 Pappalardo, L., Buono, G., Fanara, S. and Petrosino, P., 2018. Combining textural and geochemical
1450 investigations to explore the dynamics of magma ascent during Plinian eruptions: a Somma–
1451 Vesuvius volcano (Italy) case study. *Contributions to Mineralogy and Petrology*, *173*(7), pp.1-20.

1452 Parmigiani, A., Faroughi, S., Huber, C., Bachmann, O. and Su, Y., 2016. Bubble accumulation and its
1453 role in the evolution of magma reservoirs in the upper crust. *Nature*, *532*(7600), pp.492-495.

1454 Pichavant M, Poussineau S, Lesne P, Solaro C and Bourdier J (2018). Experimental Parametrization of
1455 Magma Mixing: Application to the ad 1530 Eruption of La Soufrière, Guadeloupe (Lesser
1456 Antilles). *Journal of Petrology*, 59(2), pp.257-282.

1457 Pinel, V. and Jaupart, C., 2000. The effect of edifice load on magma ascent beneath a
1458 volcano. *Philosophical Transactions of the Royal Society of London. Series A: Mathematical, Physical*
1459 *and Engineering Sciences*, *358*(1770), pp.1515-1532.

1460 Pinkerton, H., James, M. and Jones, A., 2002. Surface temperature measurements of active lava
1461 flows on Kilauea volcano, Hawai' i. *Journal of volcanology and geothermal research*, *113*(1-2),
1462 pp.159-176.

1463 Pino, N. A., Moretti, R., Allard, P., & Boschi, E. (2011). Seismic precursors of a basaltic paroxysmal
1464 explosion track deep gas accumulation and slug upraise. Journal of Geophysical Research: Solid
1465 Earth, 116(B2).

1466 Pistone, M., Caricchi, L., & Ulmer, P. (2021). CO_2 favours the accumulation of excess fluids in felsic
1467 magmas. Terra Nova, 33(2), 120-128.

1468 Portnyagin, M., Almeev, R., Matveev, S. and Holtz, F., 2008. Experimental evidence for rapid water
1469 exchange between melt inclusions in olivine and host magma. *Earth and Planetary Science*
1470 *Letters*, *272*(3-4), pp.541-552.

1471 Poussineau, S., 2005. *Dynamique des magmas andésitiques: approche expérimentale et*
1472 *pétrostructurale; application à la Soufrière de Guadeloupe et à la Montagne Pelée* (Doctoral
1473 dissertation, Université d'Orléans).

1474 Preece, K., Gertisser, R., Barclay, J., Charbonnier, S.J., Komorowski, J.C. and Herd, R.A., 2016.
1475 Transitions between explosive and effusive phases during the cataclysmic 2010 eruption of Merapi
1476 volcano, Java, Indonesia. *Bulletin of Volcanology*, *78*(8), pp.1-16.

1477 Pritchard, M. E., Mather, T. A., McNutt, S. R., Delgado, F. J., & Reath, K. (2019). Thoughts on the
1478 criteria to determine the origin of volcanic unrest as magmatic or non-magmatic. Philosophical
1479 Transactions of the Royal Society A, 377(2139), 20180008.

1480 Putirka K (2008). Thermometers and Barometers for Volcanic Systems. *Reviews in Mineralogy and*
1481 *Geochemistry*, 69(1), pp.61-120.

1482 Quareni, F., & Mulargia, F. (1993). Modeling the closure of volcanic conduits with an application to
1483 Mount Vesuvius. Journal of Geophysical Research: Solid Earth, 98(B3), 4221-4229.

1484 Quareni, F., Moretti, R., Piochi, M., & Chiodini, G. (2007). Modeling of the thermal state of Mount
1485 Vesuvius from 1631 AD to present and the role of CO2 degassing on the volcanic conduit closure
1486 after the 1944 AD eruption. Journal of Geophysical Research: Solid Earth, 112(B3).

1487 Ratdomopurbo, A., Beauducel, F., Subandriyo, J., Nandaka, I.M.A., Newhall, C.G., Sayudi, D.S. and
1488 Suparwaka, H., 2013. Overview of the 2006 eruption of Mt. Merapi. *Journal of Volcanology and*
1489 *Geothermal research*, *261*, pp.87-97.

1490 Reubi, O., Blundy, J. and Varley, N.R., 2013. Volatiles contents, degassing and crystallisation of
1491 intermediate magmas at Volcan de Colima, Mexico, inferred from melt inclusions. *Contributions to*
1492 *Mineralogy and Petrology*, *165*(6), pp.1087-1106.

1493 Robertson, R.E.A., Cole, P., Sparks, R.S.J., Harford, C., Lejeune, A.M., McGuire, W.J., Miller, A.D.,
1494 Murphy, M.D., Norton, G., Stevens, N.F. and Young, S.R., 1998. The explosive eruption of soufriere
1495 hills volcano, montserrat, west indies, 17 september, 1996. *Geophysical Research Letters*, *25*(18),
1496 pp.3429-3432.

1497 Roedder, E. (1984). Fluid Inclusions. Mineralogical Society of America, Monograph 12, , 644 p.

1498 Roggensack, K., Hervig, R.L., McKnight, S.B. and Williams, S.N., 1997. Explosive basaltic volcanism
1499 from Cerro Negro volcano: influence of volatiles on eruptive style. *Science*, *277*(5332), pp.1639-
1500 1642.

1501 Roman DC and Cashman KV (2018) Top–Down Precursory Volcanic Seismicity: Implications for
1502 'Stealth' Magma Ascent and Long-Term Eruption Forecasting. Front. Earth Sci. 6:124. doi:
1503 10.3389/feart.2018.00124

1504 Roman, D.C., LaFemina, P.C., Bussard, R., Stephens, K., Wauthier, C., Higgins, M., Feineman, M.,
1505 Arellano, S., de Moor, J.M., Avard, G. and Cruz, M.M., 2019. Mechanisms of unrest and eruption at
1506 persistently restless volcanoes: Insights from the 2015 eruption of Telica Volcano,
1507 Nicaragua. *Geochemistry, Geophysics, Geosystems*, *20*(8), pp.4162-4183.

1508 Rubin, A.E., Cooper, K.M., Till, C.B., Kent, A.J., Costa, F., Bose, M., Gravley, D., Deering, C. and Cole, J.,
1509 2017. Rapid cooling and cold storage in a silicic magma reservoir recorded in individual
1510 crystals. *Science*, *356*(6343), pp.1154-1156.

1511 Ruprecht, P. and Bachmann, O., 2010. Pre-eruptive reheating during magma mixing at Quizapu
1512 volcano and the implications for the explosiveness of silicic arc volcanoes. *Geology*, *38*(10), pp.919-
1513 922.

1514 Rutherford, M.J., 2008. Magma ascent rates. *Reviews in Mineralogy and Geochemistry*, *69*(1),
1515 pp.241-271.

Samper, A., Quidelleur, X., Komorowski, J.C., Lahitte, P. and Boudon, G., 2009. Effusive history of the grande decouverte volcanic complex, southern basse-terre (guadeloupe, french west indies) from new k–ar cassignol–gillot ages. *Journal of Volcanology and Geothermal Research*, *187*(1-2), pp.117-130.

Scaillet, B., Pichavant, M. and Cioni, R., 2008. Upward migration of Vesuvius magma chamber over the past 20,000 years. *Nature*, *455*(7210), pp.216-219.

Scandone, R., Cashman, K.V. and Malone, S.D., 2007. Magma supply, magma ascent and the style of volcanic eruptions. *Earth and Planetary Science Letters*, *253*(3-4), pp.513-529.

Schiano, P., 2003. Primitive mantle magmas recorded as silicate melt inclusions in igneous minerals. *Earth-Science Reviews*, *63*(1-2), pp.121-144.

Schleicher J and Bergantz G (2017). The Mechanics and Temporal Evolution of an Open-system Magmatic Intrusion into a Crystal-rich Magma. *Journal of Petrology*, 58(6), pp.1059-1072.

Schleicher J, Bergantz G, Breidenthal R and Burgisser A (2016). Time scales of crystal mixing in magma mushes. *Geophysical Research Letters*, 43(4), pp.1543-1550.

Schmitt, A.K., 2001. Gas-saturated crystallization and degassing in large-volume, crystal-rich dacitic magmas from the Altiplano-Puna, northern Chile. *Journal of Geophysical Research: Solid Earth*, *106*(B12), pp.30561-30578.

Semet, M., Vatin-Pérignon, N., Vincent, P.M. and Joron, J.L., 1981. L'éruption volcanique du XVI éme siècle de la Soufrière de Guadeloupe. Mélanges de magmas et dynamisme éruptif. *Bulletin PIRPSEV-CNRS*, p.42.

Shaw, A.M., Hauri, E.H., Fischer, T.P., Hilton, D.R. and Kelley, K.A., 2008. Hydrogen isotopes in Mariana arc melt inclusions: Implications for subduction dehydration and the deep-Earth water cycle. *Earth and Planetary Science Letters*, *275*(1-2), pp.138-145.

Sides, I.R., Edmonds, M., Maclennan, J., Swanson, D.A. and Houghton, B.F., 2014. Eruption style at Kīlauea Volcano in Hawai ‘i linked to primary melt composition. *Nature Geoscience*, *7*(6), pp.464-469.

Solaro C, Balcone-Boissard Hè, Morgan DJ, Boudon G, Martel C and Ostorero L (2020) A System Dynamics Approach to Understanding the deep Magma Plumbing System Beneath Dominica (Lesser Antilles). Front. Earth Sci. 8:574032. doi: 10.3389/feart.2020.574032

Sparks, R. and Cashman, K., (2017). Dynamic Magma Systems: Implications for Forecasting Volcanic Activity. *Elements*, 13(1), pp.35-40.

Sparks, R.S.J., 1997. Causes and consequences of pressurisation in lava dome eruptions. *Earth and Planetary Science Letters*, *150*(3-4), pp.177-189.

Sparks, S.R., Sigurdsson, H. and Wilson, L., 1977. Magma mixing: a mechanism for triggering acid explosive eruptions. *Nature*, *267*(5609), pp.315-318.

Sparks, R.S.J., Barclay, J., Calder, E.S., Herd, R.A., Komorowski, J-C., Norton, G.E., Ritchie, L., Voight, B., Woods, A.W. (2002) Generation of a debris avalanche and violent pyroclastic density current : the Boxing Day eruption of 26 december 1997 at the Soufrière Hills Volcano, Montserrat. In : T.H. Druitt, B.P. Kokelaar (Eds), The eruption of Soufrière Hills Volcano, Montserrat, from 1995 to 1999, Geological Society, London, Memoirs, 21, 409-434

Spera, F.J. and Bohrson, W.A., 2018. Rejuvenation of crustal magma mush: a tale of multiply nested processes and timescales. *American Journal of Science*, *318*(1), pp.90-140.

Steele-Macinnis, M., Esposito, R. and Bodnar, R.J., 2011. Thermodynamic model for the effect of post-entrapment crystallization on the H2O–CO2 systematics of vapor-saturated, silicate melt inclusions. *Journal of Petrology*, *52*(12), pp.2461-2482.

Stix, J. and de Moor, J.M., 2018. Understanding and forecasting phreatic eruptions driven by magmatic degassing. *Earth, Planets and Space*, *70*(1), pp.1-19.

Symonds, R.B., Gerlach, T.M. and Reed, M.H., 2001. Magmatic gas scrubbing: implications for volcano monitoring. *Journal of Volcanology and Geothermal Research*, *108*(1-4), pp.303-341.

Taddeucci, J., Pompilio, M. and Scarlato, P., 2004. Conduit processes during the July–August 2001 explosive activity of Mt. Etna (Italy): inferences from glass chemistry and crystal size distribution of ash particles. *Journal of Volcanology and Geothermal Research*, *137*(1-3), pp.33-54.

Thomas, M.E. and Neuberg, J.W., 2014. Understanding which parameters control shallow ascent of silicic effusive magma. *Geochemistry, Geophysics, Geosystems*, *15*(11), pp.4481-4506.

Vance, J.A., 1965. Zoning in igneous plagioclase: patchy zoning. *The Journal of Geology*, *73*(4), pp.636-651.

Venugopal, S., Schiavi, F., Moune, S., Bolfan-Casanova, N., Druitt, T. and Williams-Jones, G., 2020. Melt inclusion vapour bubbles: the hidden reservoir for major and volatile elements. *Scientific reports*, *10*(1), pp.1-14.

Villemant B., Komorowski, J.-C., Dessert C., Michel A., Crispi O., Hammouya G., Beauducel F., De Chabalier, (2014). Evidence for a new shallow magma intrusion at La Soufrière sw Guadeloupe (Lesser Antilles). Insights from long-term geochemical monitoring of halogen-rich hydrothermal fluids. *Journal of Volcanology and Geothermal Research,* 285, 247–277

Voight, B., Glicken, H., Janda, R.J. and Douglass, P.M., 1981. Catastrophic rockslide-avalanche of May 18. In: P.W. Lipman and D.R. Mullineaux (Editors), The 1980 eruptions of Mount St. Helens, Washington: U.S. Geological Survey Professional Paper 1250, p. 347-378

Voight, B., Sparks, R.S.J., Miller, A.D., Stewart, R.C., Hoblitt, R.P., Clarke, A., Ewart, J., Aspinall, W.P., Baptie, B., Calder, E.S. and Cole, P., 1999. Magma flow instability and cyclic activity at Soufriere Hills volcano, Montserrat, British West Indies. *Science*, *283*(5405), pp.1138-1142.

Wadge, G., Voight, B., Sparks, R.S.J., Cole, P.D., Loughlin, S.C. and Robertson, R.E.A., 2014. An overview of the eruption of Soufriere Hills Volcano, Montserrat from 2000 to 2010. *Geological Society, London, Memoirs*, *39*(1), pp.1-40.

Wallace, P.J., 2005. Volatiles in subduction zone magmas: concentrations and fluxes based on melt inclusion and volcanic gas data. *Journal of volcanology and Geothermal Research*, *140*(1-3), pp.217-240.

Wilson, Lionel, R. Stephen J. Sparks, and George PL Walker. "Explosive volcanic eruptions—IV. The control of magma properties and conduit geometry on eruption column behaviour." *Geophysical Journal International* 63, no. 1 (1980): 117-148.

Zellmer GF, Sparks RSJ, Hawkesworth CJ and Wiedenbeck M (2003). Magma emplacement and remobilisation timescales beneath Montserrat: insights from Sr and Ba zonation in plagioclase phenocrysts. Journal of Petrology 44, 1413–1431.

Zimanowski, B., Büttner, R., Dellino, P., White, J.D. and Wohletz, K.H., 2015. Magma–water interaction and phreatomagmatic fragmentation. In *The encyclopedia of volcanoes* (pp. 473-484). Academic Press.

Zlotnicki, J., G. Boudon, and J.-L. L. Mouël (1992). The volcanic activity of La Soufrière de Guadeloupe (lesser antilles): structural and tectonic implications. *Journal of Volcanology*

Table 1: Summary of groundmass glass and microlites for each eruption.

Table 1							
Eruption	**Style**	**VEI**	**Glass**	**Microlites**	**Microlite size (µm)**	**Vesicles**	**Microlite vol%**
1657 Cal. CE	Vulcanian	2	Homogenous	subhedral - euhedral	<10	yes	18
1530 Cal. CE	Sub-Plinian	3	Heterogeneous	subhedral - euhedral	<50	yes	17-34
1010 Cal. CE	Plinian	4	Homogenous	anhedral	<5	yes	8
5680 Cal. BCE	Plinian	4	Homogenous	anhedral - subhedral	1 - 15	yes	47

Table 2: Full normalised MI dataset including major elements from EMPA and volatile data from EMPA and SIMS (*). Also shown are the enstatite (En) and anorthite (An) content of the host mineral and the calculated Kd value. Some volatiles were less than the detection limit (<dl).

Table 2																		
Eruption	**Sample**	**Host Crystal En**	**Host Crystal An**	**SiO_2**	**TiO_2**	**Al_2O_3**	**FeO**	**MnO**	**MgO**	**CaO**	**Na_2O**	**K_2O**	**F**	**S**	**Cl**	**H_2O**	**CO_2**	**δD**	**Kd**
1657 CE	0913D-pyx7-1	0.39	-	77.74	0.38	12.19	2.50	0.02	0.47	2.05	2.12	2.53	<dl	0.037	0.16	-	-	-	0.23
1657 CE	0913D-pyx7-2	0.39	-	76.72	0.39	12.24	3.14	0.12	0.54	2.38	2.40	2.07	<dl	0.019	0.18	-	-	-	0.24
1657 CE	0913D-pyx7-3	0.39	-	77.01	0.42	12.46	2.94	0.08	0.49	2.45	2.27	1.87	<dl	0.028	0.19	-	-	-	0.22
1657 CE	0913D-pyx-9-1	0.57	-	75.30	0.47	12.70	3.44	0.18	0.65	2.71	2.74	1.80	<dl	0.056	0.25	-	-	-	0.24
1657 CE	0913D-pyx16-1	0.39	-	74.79	0.43	13.58	2.76	0.03	0.86	3.33	2.45	1.76	0.051*	0.006*	0.29*	3.6*	530*	-10.1	0.28
1657 CE	0913D-pyx16-2	0.38	-	75.23	0.45	13.59	2.91	0.09	0.45	3.02	2.50	1.77	0.050*	0.005*	0.24*	3.7*	674*	-25.6	0.24
1657 CE	0913D-pyx-16-3	0.39	-	75.26	0.43	13.57	3.05	0.12	0.53	3.22	2.32	1.49	0.048*	0.005*	0.23*	3.6*	451*	-10.9	0.24
1657 CE	0913D-plg7-1	-	0.68	76.33	0.50	13.97	2.15	0.11	0.28	2.73	1.84	2.09	0.048*	0.005*	0.24*	3.4*	146*	-10.5	0.08
1657 CE	0913D-plg7-2	-	0.66	76.94	0.45	13.56	2.33	0.11	0.39	2.72	1.57	1.94	0.049*	0.006*	0.25*	3.9*	165*	-46.1	0.10
1657 CE	0913D-plg11-2	-	0.68	74.97	0.75	14.23	2.14	0.10	0.33	3.10	2.71	1.67	0.039*	0.006*	0.21*	2.4*	35*	-40.3	0.07
1657 CE	0913D-plg11-3	-	0.70	74.22	0.60	13.80	1.99	0.08	0.35	3.44	3.41	2,12	0.045*	0.007*	0.32*	3.7*	122*	-37.1	0.05

1657 CE	0913D-plg5-2	-	0.69	73.13	0.53	12.50	4.67	0.14	0.87	3.06	2.97	2.11	0.046*	0.009*	0.36*	3.9*	192*	-26.6	0.05
1657 CE	0913D-plg2-1	-	0.75	75.90	0.45	13.90	2.05	0.01	0.31	2.73	3.29	1.37	0.04*	0.003*	0.19*	2.3*	253*	-43.6	0.06
1657 CE	0913D-plg3-1	-	0.29	74.49	0.57	13.13	3.88	0.08	0.79	2.60	2.33	2.13	<dl	<dl	0.32	-	-	-	0.06
1657 CE	0913D-plg3-2	-	0.97	74.98	0.55	12.70	4.28	0.15	0.76	2.85	1.68	2.04	<dl	0.021	0.33	-	-	-	0.07
1657 CE	0913D-plg3-3	-	0.97	74.82	0.60	12.51	3.78	0.13	0.76	2.96	2.22	2.24	<dl	0.015	0.30	-	-	-	0.07
1657 CE	0913D-plg3-4	-	0.57	74.71	0.64	12.47	3.77	0.12	0.77	2.74	2.53	2.24	<dl	0.025	0.32	-	-	-	0.05
1657 CE	0913D-plg1-1	-	0.58	75.69	0.56	12.55	3.29	0.04	0.58	2.63	2.53	2.13	<dl	0.007*	0.29*	2.4*	35*	-39.4	0.08
1657 CE	0913D-plg1-2	-	0.76	75.37	0.58	12.49	3.37	0.07	0.59	2.72	2.62	2.19	<dl	0.036	0.29	-	-	-	0.05
1657 CE	0913D-plg5-1	-	0.66	74.94	0.53	13.42	4.69	0.16	0.80	3.04	0.82	1.59	0.05*	0.009*	0.36*	4.1*	36*	-50.8	0.05
1657 CE	0913D-plg1-3	-	0.69	74.66	0.46	13.07	3.29	0.13	0.56	3.06	2.64	213	<dl	0.021	0.272	-	-	-	0.06
1657 CE	0913D-plg5A-1	-	0.59	76.20	0.31	13.11	2.44	0.01	0.34	2.75	2.59	2.25	<dl	0.010	0.221	-	-	-	0.07
1657 CE	0913D-plg5A-2	-	0.61	75.94	0.34	13.51	2.28	0.10	0.32	3.00	2.41	2.10	<dl	0.042	0.089	-	-	-	0.09
1657 CE	0913D-plg8-1	-	0.57	77.61	0.48	12.36	2.38	0.02	0.39	2.28	2.31	2.17	<dl	<dl	0.225	-	-	-	0.07
1657 CE	0913D-plg8-2	-	0.58	78.16	0.55	12.43	1.78	0.10	0.39	2.11	2.36	2.12	<dl	0.022	0.211	-	-	-	0.07
1657 CE	0913D-plg4-1	-	0.59	77.12	0.59	12.34	2.44	0.12	0.42	2.47	2.47	2.03	<dl	<dl	0.208	-	-	-	0.07
1657 CE	0913D-plg4-2	-	0.59	77.31	0.59	12.25	2.42	0.17	0.35	2.27	2.54	2.09	<dl	0.017	0.196	-	-	-	0.06
1657 CE	0913D-plg4-3	-	0.59	77.75	0.51	12.34	2.16	0.04	0.33	2.27	2.61	1.99	<dl	0.010	0.187	-	-	-	0.06
1657 CE	0913D-plg4-4	-	0.59	77.46	0.53	12.25	2.48	0.13	0.34	2.31	2.49	2.02	<dl	<dl	0.201	-	-	-	0.06
1657 CE	0913D-plg4-5	-	0.59	77.77	0.53	12.36	2.24	0.03	0.35	2.49	2.17	2.06	<dl	<dl	0.201	-	-	-	0.08
1657 CE	0913D-plg4-6	-	0.59	77.65	0.53	12.20	2.25	0.10	0.34	2.33	2.51	2.10	<dl	0.017	0.199	-	-	-	0.05
1657 CE	0913D-plg6-1	-	0.64	77.28	0.50	12.85	2.05	0.02	0.27	2.25	2.43	2.35	<dl	<dl	0.194	-	-	-	0.05
1657 CE	0913D-plg6-2	-	0.67	76.37	0.51	13.24	2.07	0.05	0.28	2.69	2.61	2.17	<dl	0.026	0.182	-	-	-	0.06
1010 CE	0924A-pyx1A-3	0.56	-	69.50	0.67	14.77	5.36	0.21	0.99	3.75	3.13	1.62	<dl	<dl	0.20	-	-	-	0.24
1010 CE	0924A-pyx1D-1	0.56	-	69.87	0.66	14.53	5.03	0.18	0.93	3.90	3.25	1.65	<dl	0.065	0.20	-	-	-	0.24
1010 CE	0924A-pyx1D-2	0.56	-	70.33	0.64	14.46	5.07	0.14	0.89	3.53	3.27	1.69	<dl	0.022	0.21	-	-	-	0.23
1010 CE	0924A-pyx1D-4	0.59	-	70.66	0.61	14.49	4.57	0.10	0.92	3.62	3.20	1.83	0.035*	0.006*	0.2*	2.2*	11*	-29.5	0.23
1010 CE	0924A-pyx1G-1	0.57	-	69.66	0.67	14.79	4.98	0.14	0.91	3.98	3.37	1.50	<dl	0.046	0.19	-	-	-	0.23
1010 CE	0924A-pyx1G-4	0.57	-	70.30	0.45	14.51	5.12	0.08	0.93	4.00	3.18	1.43	<dl	0.012	0.19	-	-	-	0.23
1010 CE	0924A-pyx2C-1	0.57	-	69.51	0.57	14.69	5.28	0.12	1.03	3.81	3.46	1.53	<dl	0.042	0.21	-	-	-	0.24
1010 CE	0924A-pyx2C-2	0.56	-	70.41	0.52	14.36	4.84	0.09	0.88	3.87	3.47	1.56	<dl	0.031	0.19	-	-	-	0.22
1010 CE	0924A-pyx1B-1	0.41	-	70.80	0.55	14.50	4.86	0.23	0.85	3.80	2.87	1.55	<dl	0.015	0.21	-	-	-	0.25
1010 CE	0924A-pyx13-2	0.60	-	73.28	0.65	14.36	4.90	0.10	1.01	3.19	1.08	1.44	0.041*	0.006*	0.16*	<dl	<dl	-	0.23

1010 CE	0111A-pyx10-2	0.57	-	73.85	0.53	15.43	3.67	0.07	0.68	3.92	0.51	1.33	0.043*	0.01*	0.18*	3.3*	60*	-34.5	0.22
1010 CE	0924A-pyx2F-1	0.54	-	64.32	0.31	21.31	2.34	0.04	0.38	7.04	3.16	1.11	<dl	0.006	<dl	-	-	-	0.25
1010 CE	0111A-pyx10-1	0.57	-	73.44	0.77	15.74	3.63	0.14	0.28	4.04	0.80	1.15	0.048*	0.02	0.24*	4.4*	122*	-30.5	0.22
1010 CE	0924A-pyx6-1	0.61	-	70.28	0.58	15.35	5.28	0.12	0.92	3.47	2.76	1.24	0.042*	0.01*	0.15*	2.8*	131*	-34.5	0.23
1010 CE	0924A-plg2E-1	-	0.67	73.25	0.57	13.92	4.04	0.16	0.78	3.18	2.25	1.85	<dl	0.020	0.17	-	-	-	0.09
1010 CE	0924A-plg2E-2	-	0.67	72.50	0.44	14.12	3.55	0.10	0.77	3.48	3.26	1.77	<dl	0.023	0.16	-	-	-	0.07
1010 CE	0924A-plg2E-3	-	0.60	72.68	0.54	14.04	3.85	0.05	0.83	3.25	2.85	1.92	<dl	0.031	0.18	-	-	-	0.10
1010 CE	0924A-plg2B-1	-	0.62	75.52	0.49	12.41	2.90	0.06	0.48	2.51	3.36	2.26	<dl	0.039	0.32	-	-	-	0.05
1010 CE	0924A-plg2B-2	-	0.61	75.08	0.63	12.57	2.86	0.00	0.42	2.69	3.35	2.39	<dl	0.025	0.29	-	-	-	0.06
1010 CE	0924A-plg2A-1	-	0.61	77.47	0.37	12.28	2.54	0.08	0.34	2.22	2.30	2.39	<dl	0.010	0.25	-	-	-	0.06
5680 BCE	1101viA-pyx2E-2	0.64	-	64.62	0.79	16.08	8.19	0.17	2.75	6.43	0.24	0.73	<dl	0.08	0.17	-	-	-	0.30
5680 BCE	1101viA-pyx2E-3	0.65	-	66.18	0.72	14.76	7.16	0.12	2.50	4.35	3.09	1.12	<dl	0.02	0.21	-	-	-	0.30
5680 BCE	1101viA-pyx2E-4	0.62	-	66.74	0.61	14.79	6.94	0.16	2.54	4.53	2.50	1.18	<dl	0.04	0.20	-	-	-	0.36
5680 BCE	1101viA-pyx2F-3	0.55	-	76.49	0.55	13.34	4.09	0.08	0.87	2.99	0.09	1.49	<dl	<dl	0.22	-	-	-	0.29
5680 BCE	1101viA-pyx1-1	0.58	-	69.38	0.44	13.77	8.03	0.28	1.00	4.24	1.56	1.32	0.048*	0.02*	0.23*	4.2*	866*	-59	0.26
5680 BCE	1101viA-pyx1-2	0.56	-	69.54	0.47	14.76	6.62	0.31	0.81	4.16	1.88	1.46	0.044*	0.02*	0.19*	3.5*	448*	-33.1	0.25
5680 BCE	1101viA-pyx2A-2	0.37	-	76.41	0.49	12.77	4.25	0.17	1.13	3.50	0.05	1.24	<dl	0.02	0.26	-	-	-	0.31
5680 BCE	1101viA-pyx2A-1	0.34	-	75.01	0.55	12.38	3.88	0.13	0.87	3.40	1.62	2.17	<dl	0.02	0.13	-	-	-	0.25
5680 BCE	1101viA-pyx2B-3	0.37	-	74.93	0.59	13.46	4.00	0.10	0.91	3.45	0.92	1.63	<dl	0.05	0.23	-	-	-	0.26
5680 BCE	1101viA-pyx2E-1	0.64	-	64.88	0.64	15.40	7.04	0.20	2.84	4.71	312	1.17	<dl	0.03	0.23	-	-	-	0.36
5680 BCE	1101viA-pyx5-1	0.62	-	68.67	0.82	17.01	3.49	0.22	0.63	4.74	3.03	1.38	0.043*	0.02*	0.19*	3.4*	129*	-64.8	0.35
5680 BCE	1101viA-pyx5-2	0.59	-	64.68	1.00	17.54	7.55	0.15	1.22	6.65	008	1.13	0.051*	0.02*	0.2*	3.1*	182*	-50.8	0.23
5680 BCE	1101viA-plg1D-1	-	0.69	76.13	0.34	14.17	3.02	0.12	0.38	2.75	1.22	1.87	0.06*	0.003*	0.14*	2.4*	116*	-33.2	0.12
5680 BCE	1101viA-plg1D-2	-	0.73	75.61	0.49	12.85	2.59	0.14	0.47	3.02	2.78	2.06	<dl	0.01	0.24	-	-	-	0.04
5680 BCE	1101viA-plg1D-3	-	0.67	76.68	0.51	12.93	2.83	0.07	0.48	2.79	1.66	2.04	<dl	0.02	0.23	-	-	-	0.09
5680 BCE	1101viA-plg1C-3	-	0.77	76.39	0.50	13.41	2.91	0.06	0.43	2.86	1.46	1.99	<dl	0.01	0.25	-	-	-	0,06
5680 BCE	1101viA-plg1C-3	-	0.68	76.63	0.37	13.36	2.82	0.07	0.40	2.84	1.46	2.04	<dl	0.01	0.21	-	-	-	0.10
5680 BCE	1101viA-plg1A-1	-	0.01	75.68	0.64	12.84	3.14	0.23	0.55	2.86	2.09	1.98	<dl	0.02	0.22	-	-	-	0.07
5680 BCE	1101viA-plg1A-2	-	0.68	76.27	0.70	12.73	3.36	0.01	0.56	2.87	1.62	1.88	<dl	0.02	0.24	-	-	-	0.09
5680 BCE	1101viA-plg1E-2	-	0.70	74.97	0.42	13.72	2.75	0.02	0.43	3.36	2.41	1.90	<dl	<dl	0.21	-	-	-	0.07
5680 BCE	1101viA-plg1B-1	-	0.67	76.25	0.48	13.12	3.27	0.09	0.46	2.87	1.57	1.90	<dl	0.01	0.18	-	-	-	0.10
5680 BCE	1101viA-plg1B-2	-	0.66	76.33	0.47	12.93	3.60	0.04	0.47	2.98	141	1.77	<dl	<dl	0.10	-	-	-	0.12

5680 BCE	1101viA-plg1B-3	-	0.71	73.31	0.57	12.28	3.73	0.03	1.42	3.88	2.89	1.90	<dl	0.02	0.13	-	-	-	0.06

1622

1623 **Table 3:** Summary table of the analysed data and calculated properties (including temperature for MI and GM, pressure and viscosity (GM without
1624 microlites and GM+X with microlites) *Boudon et al., 2008; Pichavant et al., 2018; Poussineau, 2005

Table 3

Eruption	Eruption Style	VEI	Measured Properties					Calculated Properties						
			Av. Bulk Rock SiO_2 (wt%)	Av. MI SiO_2 (wt%)	Max. H_2O (wt%)	Max. CO_2 (ppm)	Microlites (vol%)	Av. MI Temp (°C)	Av. GM Temp (°C)	Pressure (MPa)	Depth (Km)	Viscosity (Pa·s)		Ascent Rate (m/s)
												GM	GM+X	
1657 Cal. CE	Vulcanian	2-3	58.1	76.1	4.14	674	18	1000	975	190	7.7	$10^{7.6}$	10^{8}	0.7 - 3
1530 Cal. CE	Sub-Plinian	3	57.5*	74.3*	5*	-	17 - 34	875*	1000*	170*	7*	$10^{8.2}$	$10^{8.5}$	2 - 4
1010 Cal. CE	Plinian	4	58	71.6	4.42	131	8	1000	1025	210	8.6	10^{6}	10^{6}	0.6 - 12
5680 Cal. BCE	Plinian	4	-	72.7	4.19	866	47	1035	990	220	8.7	$10^{5.4}$	10^{7}	0.04 - 1

1625

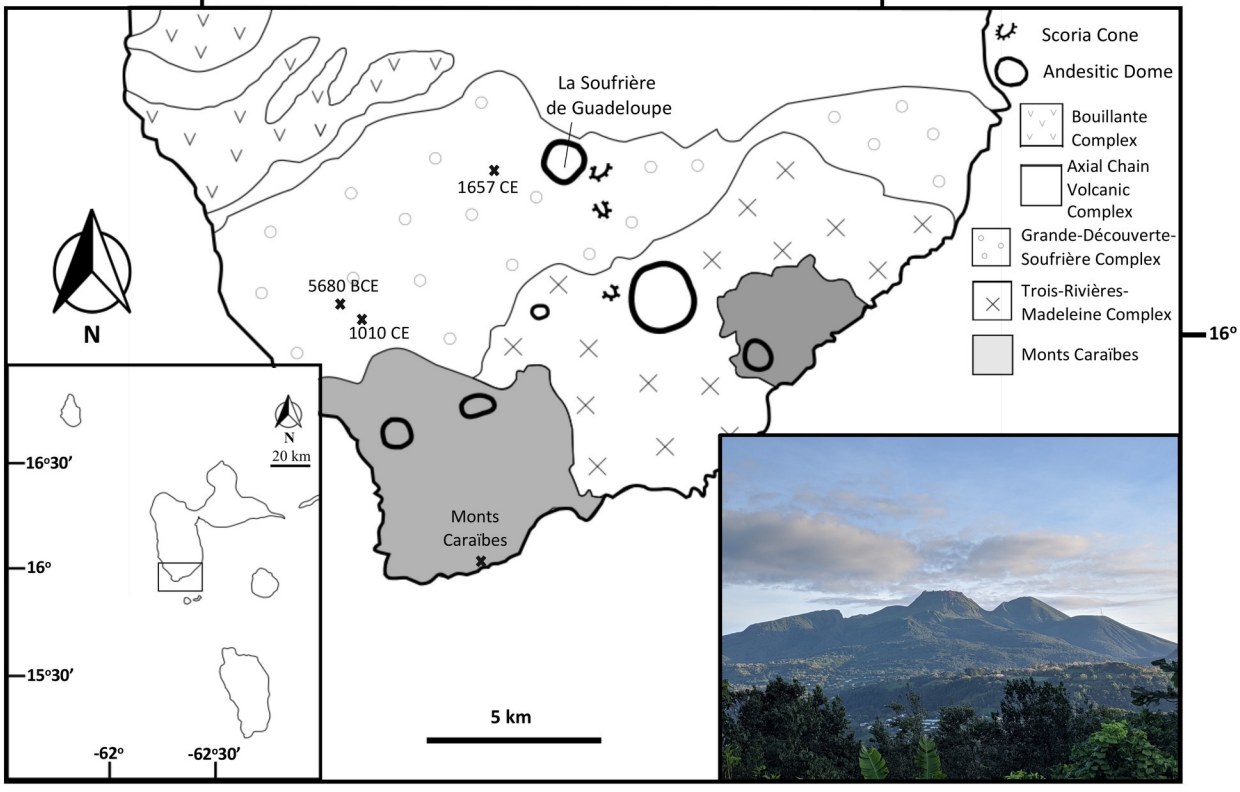
-61°45′
-61°35′
16°
Scoria Cone
Andesitic Dome
Bouillante Complex
Axial Chain Volcanic Complex
Grande-Découverte-Soufrière Complex
Trois-Rivières-Madeleine Complex
Monts Caraïbes
La Soufrière de Guadeloupe
1657 CE
5680 BCE
1010 CE
N
Monts Caraïbes
5 km
N
20 km
16°30′
16°
15°30′
-62°
-62°30′

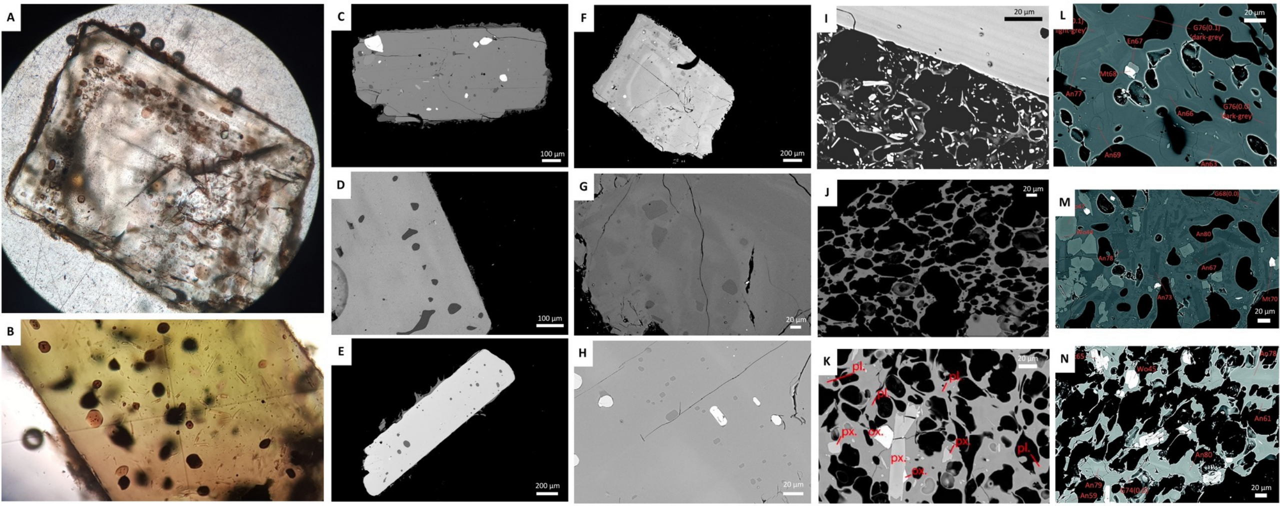
A
B
C
100 µm
D
100 µm
E
200 µm
F
200 µm
G
20 µm
H
20 µm
I
20 µm
J
20 µm
K
20 µm
pl.
pl.
pl.
px.
ox.
px.
px.
ox.
pl.
L
20 µm
'light-grey'
G76(0.1)
'dark-grey'
En67
Mt68
An77
An66
'dark-grey'
An69
An63
M
G68(0.0)
Wo44
An80
An78
An67
An73
Mt70
20 µm
N
Wo45
An78
An61
An80
An79
An59
20 µm

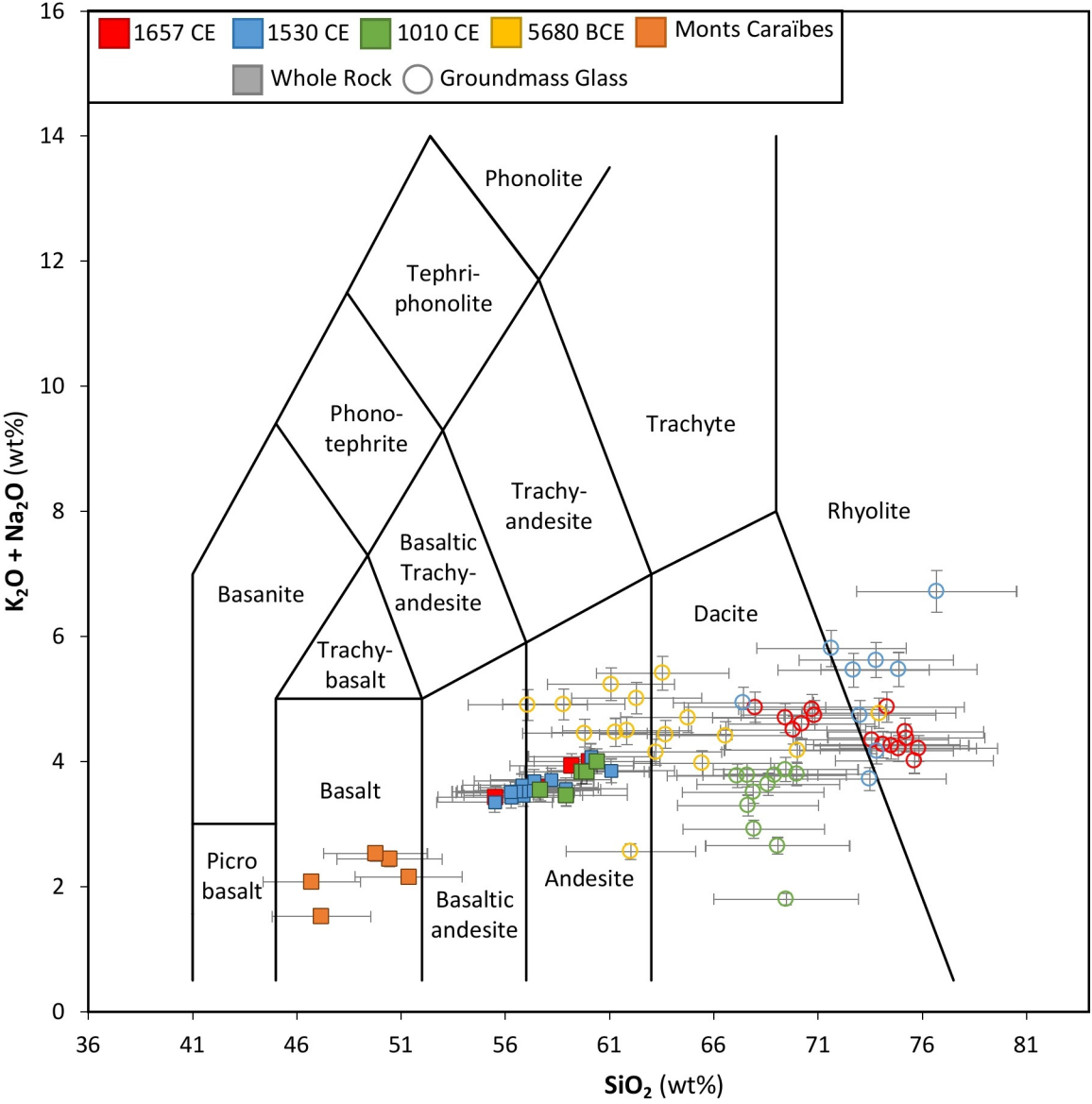
1657 CE
1530 CE
1010 CE
5680 BCE
Monts Caraïbes
Whole Rock
Groundmass Glass
Phonolite
Tephri-phonolite
Phono-tephrite
Trachyte
Trachy-andesite
Rhyolite
Basaltic Trachy-andesite
Basanite
Dacite
Trachy-basalt
Basalt
Picro basalt
Andesite
Basaltic andesite
$K_2O + Na_2O$ (wt%)
SiO_2 (wt%)
0
2
4
6
8
10
12
14
16
36
41
46
51
56
61
66
71
76
81

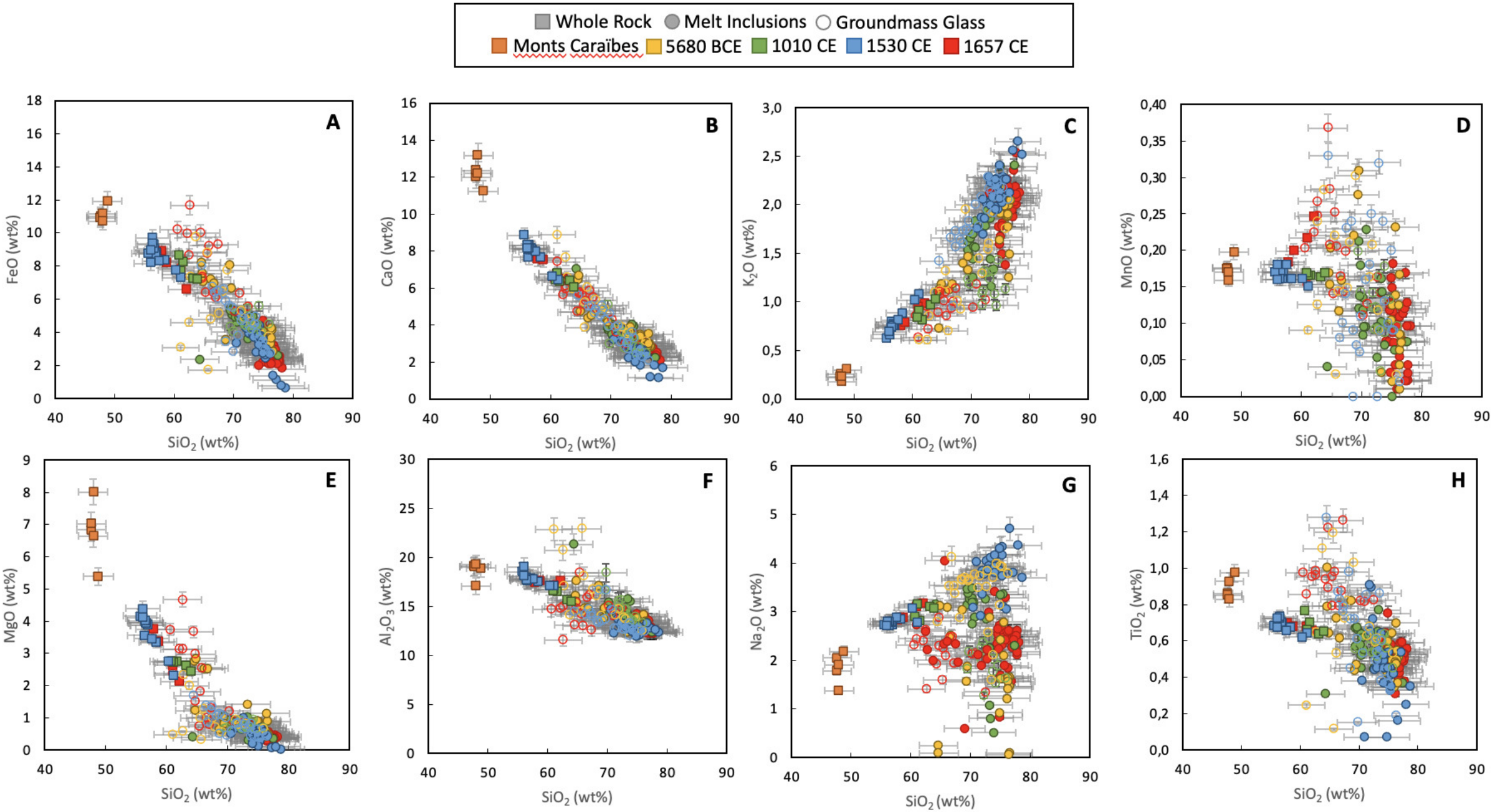
Whole Rock
Melt Inclusions
Groundmass Glass
Monts Caraïbes
5680 BCE
1010 CE
1530 CE
1657 CE
A
FeO (wt%)
SiO2 (wt%)
B
CaO (wt%)
SiO2 (wt%)
C
K2O (wt%)
SiO2 (wt%)
D
MnO (wt%)
SiO2 (wt%)
E
MgO (wt%)
SiO2 (wt%)
F
Al2O3 (wt%)
SiO2 (wt%)
G
Na2O (wt%)
SiO2 (wt%)
H
TiO2 (wt%)
SiO2 (wt%)

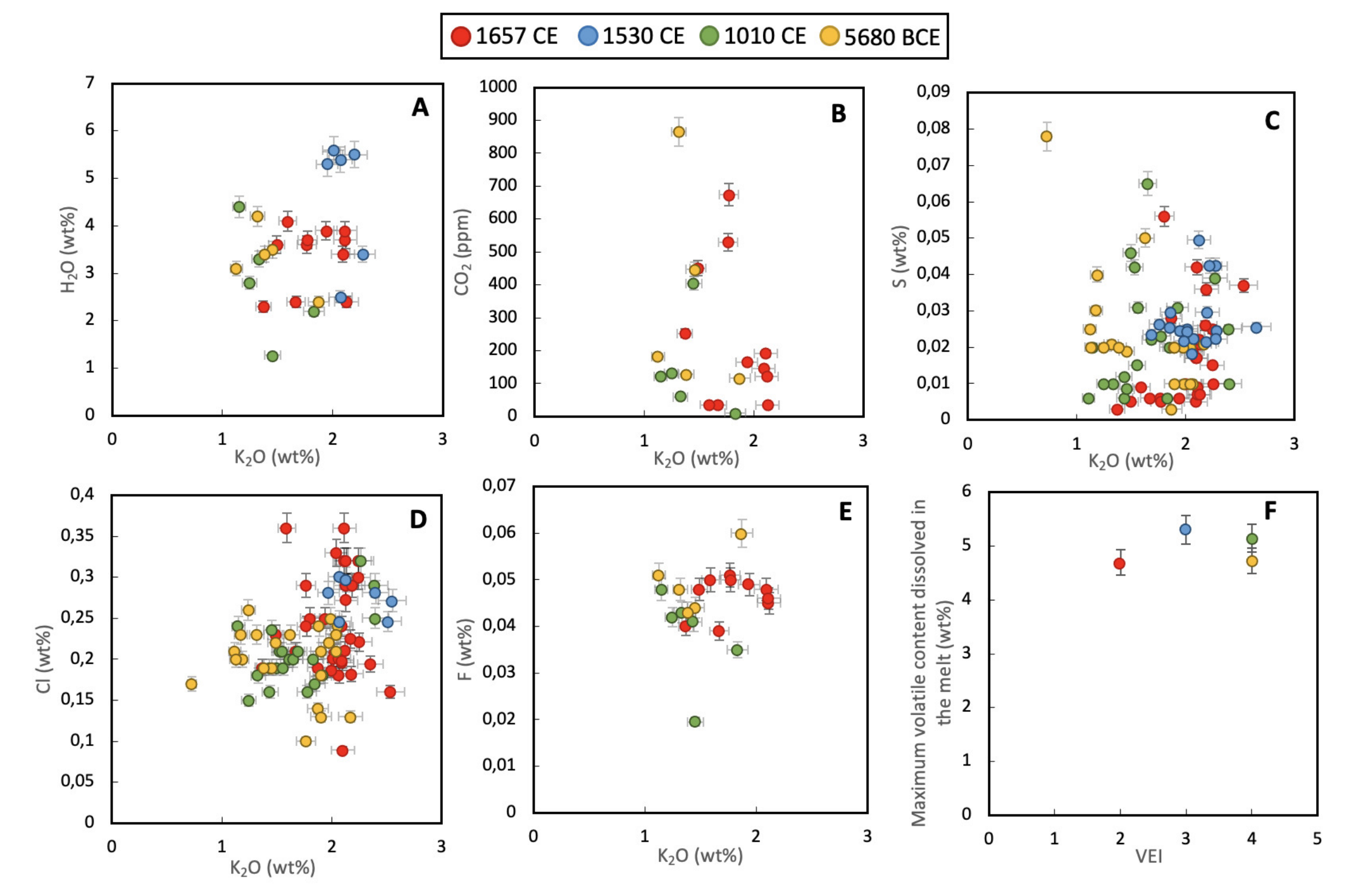
1657 CE
1530 CE
1010 CE
5680 BCE
A
B
C
D
E
F
H2O (wt%)
CO2 (ppm)
S (wt%)
Cl (wt%)
F (wt%)
K2O (wt%)
Maximum volatile content dissolved in the melt (wt%)
VEI

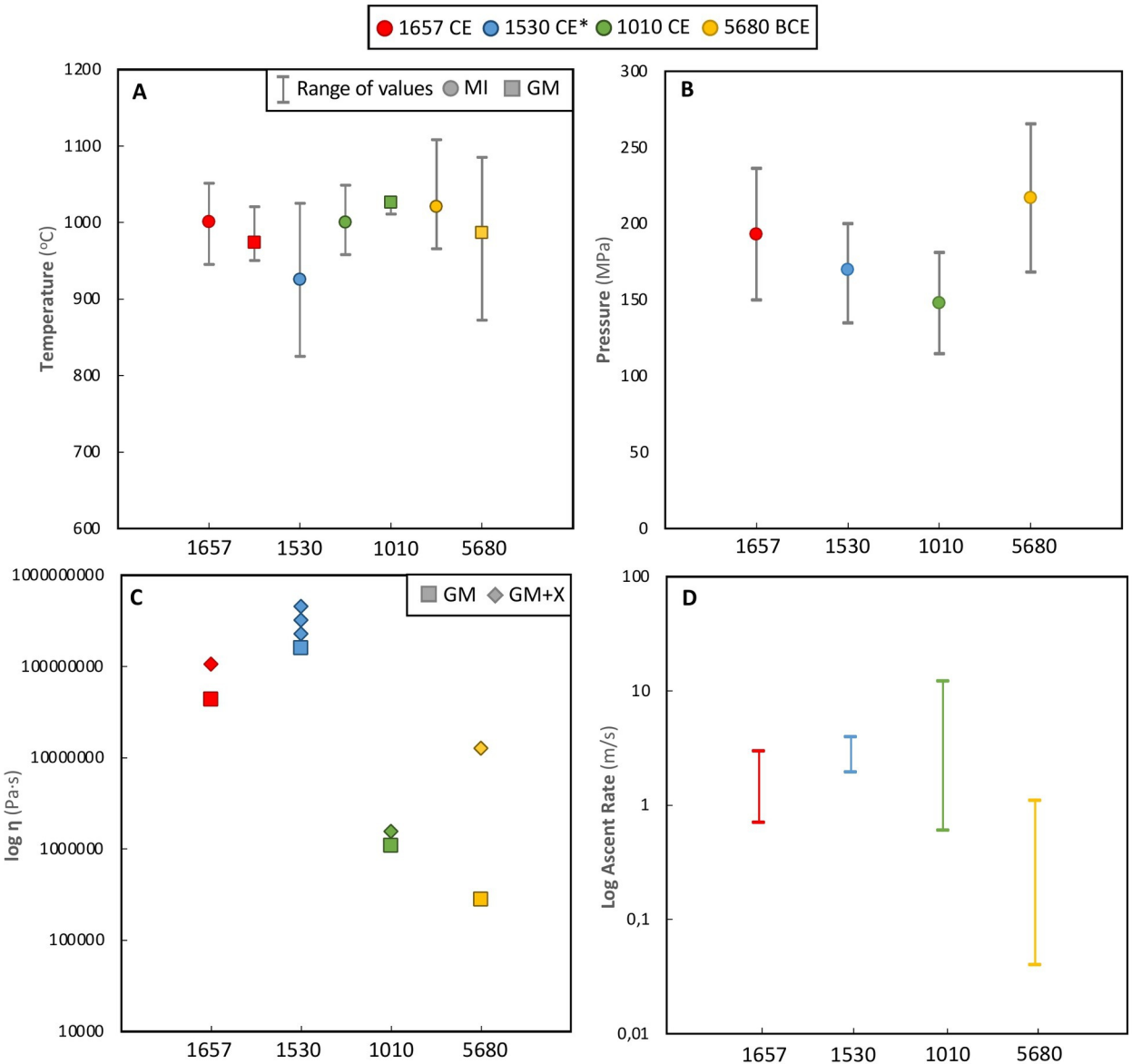
1657 CE
1530 CE*
1010 CE
5680 BCE
A
Range of values
MI
GM
Temperature (°C)
1200
1100
1000
900
800
700
600
1657
1530
1010
5680
B
Pressure (MPa)
300
250
200
150
100
50
0
C
GM
GM+X
log η (Pa·s)
1000000000
100000000
10000000
1000000
100000
10000
D
Log Ascent Rate (m/s)
100
10
1
0,1
0,01

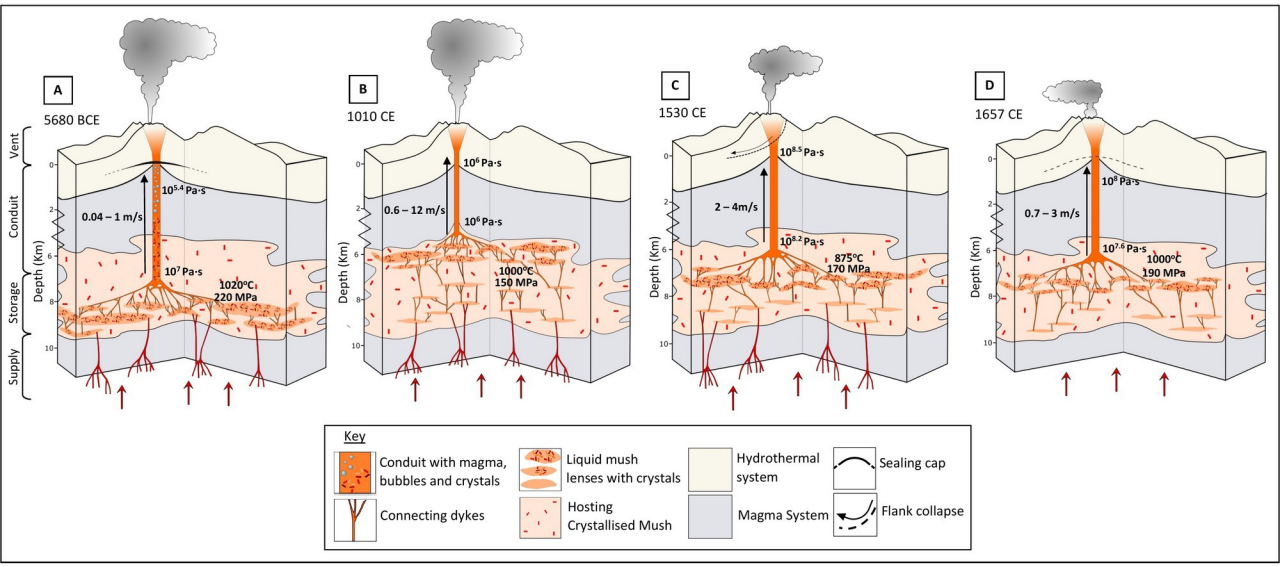
A
5680 BCE
B
1010 CE
C
1530 CE
D
1657 CE
Vent
Conduit
Storage
Supply
Depth (Km)
0
2
6
8
10
$10^{5.4}$ Pa·s
0.04 – 1 m/s
10^{7} Pa·s
1020°C
220 MPa
10^{6} Pa·s
0.6 – 12 m/s
10^{6} Pa·s
1000°C
150 MPa
$10^{8.5}$ Pa·s
2 – 4m/s
$10^{8.2}$ Pa·s
875°C
170 MPa
10^{8} Pa·s
0.7 – 3 m/s
$10^{7.6}$ Pa·s
1000°C
190 MPa
Key
Conduit with magma, bubbles and crystals
Connecting dykes
Liquid mush lenses with crystals
Hosting Crystallised Mush
Hydrothermal system
Magma System
Sealing cap
Flank collapse